QUANTUM DYNAMICS IN ULTRACOLD RYDBERG ATOMIC GASES

A thesis submitted towards partial fulfillment of the
BS-MS Dual Degree Programme

by

SAGARIKA BASAK
Reg. No. 20121008
Indian Institute of Science Education and Research, Pune
Department of Physics

under the guidance of

DR. REJISH NATH
Assistant Professor
Indian Institute of Science Education and Research, Pune

Date of Thesis Submission: March 20, 2017

Indian Institute of Science Education and Research, Pune

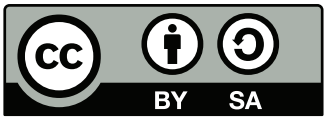

Certificate

This is to certify that this thesis entitled **Quantum dynamics in ultracold Rydberg atomic gases** towards the partial fulfillment of the BS–MS dual degree programme at the Indian Institute of Science Education and Research, Pune represents study/work carried out by **Ms. Sagarika Basak** at **IISER Pune**, under the supervision of **Dr. Rejish Nath, Assistant Professor, Department of Physics** during the academic year **2016–2017**.

DR. REJISH NATH
Assistant Professor

Pune
March 20, 2017

SAGARIKA BASAK
Reg. No. 20121008

Pune
March 20, 2017

Declaration

I hereby declare that the matter embodied in the report entitled **Quantum dynamics in ultracold Rydberg atomic gases** is the result of the work carried out by me at the **Department of Physics, Indian Institute of Science Education and Research (IISER), Pune**, under the supervision of **Dr. Rejish Nath** and the same has not been submitted elsewhere for any other degree.

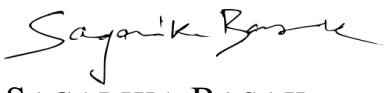

SAGARIKA BASAK — Pune

Reg. No. 20121008 — March 20, 2017

DR. REJISH NATH — Pune

Assistant Professor — March 20, 2017

Acknowledgments

I thank Dr. Rejish Nath for his guidance and for shaping me into an AMO physicist. Since I joined his Theoretical Atom Optics Group in 2013, I have not only been educated about the realm of ultracold Rydberg physics, but also learned how to conduct research with a larger goal in mind. He has always encouraged independence in thought and I am grateful for that, and for the enjoyable and fruitful discussions on the various problems we have worked on. Another major impact he has had, is taking me out of my preferred cocoon of solitude, by extolling the virtues of communication and collaboration. I am most grateful to him for how quickly I am developing the necessary skills required by a researcher.

I thank the INSPIRE SHE programme by the Department of Science and Technology, for the luxury of pursuing research and academics without worrying about an empty belly.

I thank the Director, IISER Pune and the Dean (Graduate Studies), IISER Pune for the amenities provided by the institute to facilitate my studies here.

I thank Dr. Umakant Rapol, Assistant Professor, IISER Pune for his graciousness in supervising my project as Thesis Advisory Committee member.

I thank my parents and Arshad for being there for me, always.

Finally, I thank all my teachers.

Contents

List of Figures

Dedicated to the memory of

স্বপ্ন পিসি

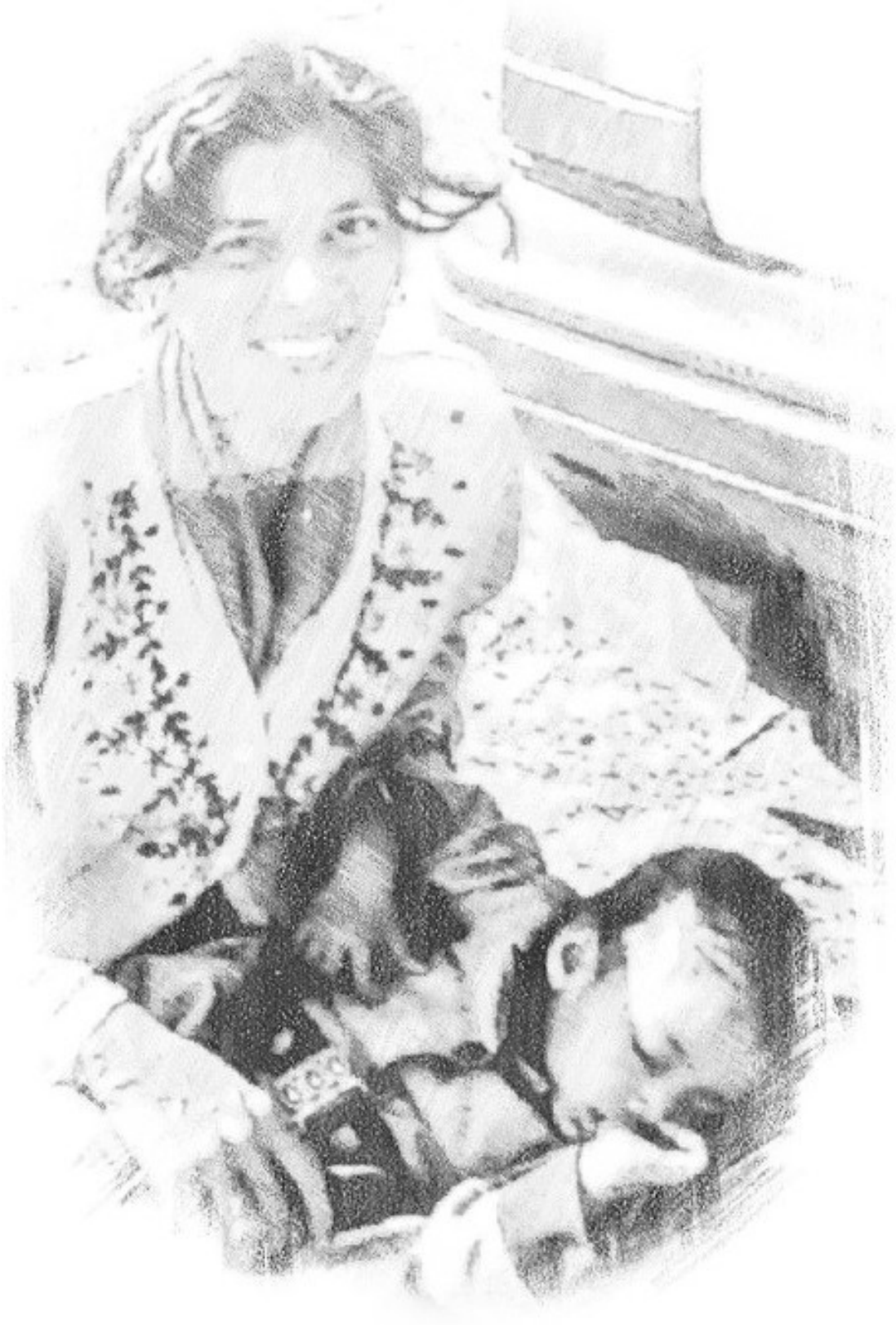

Abstract

QUANTUM DYNAMICS IN ULTRACOLD RYDBERG ATOMIC GASES

SAGARIKA BASAK

Engineering interactions in ultracold atomic systems is the primary focus of AMO physics in the recent times, which opens up various possibilities to explore exotic quantum many-body phases. Ultracold Rydberg AMO provides us with a wide scope of research. We can manipulate the existing systems to form new systems having exciting dynamics. A two-level atom is well explored when studying its interaction with a classical field, but if we adjust the system to increase the number of atoms and make them interact, we attain different and interesting dynamics. One can even adjust it to change the classical field to quantized, leading to novel dynamics. In this thesis, we explore different aspects of the two-level scheme, from single atom – light dynamics to many-atoms – light dynamics. We also explore quantized field and compare the definitions of basic parameters such as blockade radius in a quantized field to that in a classical field. For the purpose of two-level scheme, we develop our studies using the time-dependent Schrödinger equation for non-dissipative systems to the master equation for dissipative systems. In addition to the two-level scheme, we touch upon the three-level scheme and four-level scheme, studying the exotic nature of the effective interaction curve in these systems. For the purpose of the three-level and four-level scheme, we limit our analysis to numerical solutions of the master equation. Our goal is to explore different aspects of AMO ultracold physics in the realm of Rydberg atoms. We have attained interesting and novel dynamics in few-body systems and many-body systems while studying the two-level scheme. We have also attained interesting results while studying effective interactions in three-level and four-level scheme. This thesis opens up new directions of research such as attaining a potential system for exploring the collapse and revival behavior and studying entanglement, or extending the Jaynes-Cummings model to many atoms system and getting new dynamics. It even acts as a motivation for considering three-body interactions for three-level atoms.

1

Introduction

Ultracold physics challenges us in understanding and applying the counter-intuitive theorems of quantum mechanics as well as simultaneously providing us with a tool to study the system in greater detail, by lowering its temperature to a point where it can be controlled and tweaked as per desire. This level of control helps inspect the system with much ease and in much detail. Over the years, studying interactions in ultracold atomic and molecular gases is gaining importance as they provide powerful insights into many-body physics. Interesting examples are superfluid Mott insulator transition, BEC-BCS crossover, and Ising model. There are various kinds of interactions (Coulombic, van der Waals, dipolar, among others) found in atomic or molecular gases. Quantum engineering of such interactions in atomic and molecular gases, the future of atomic and molecular optical physics, will open up a platform for us to study exotic quantum many-body phases and studying and uncovering applications in quantum information protocols.

Contents

1.1 Ultracold Rydberg Atoms

Along these lines, instead of working with regular atoms, studying ultracold Rydberg atoms can be much more interesting. Rydberg atoms are atoms with valence electrons in a Rydberg state. A Rydberg state is defined by a high principal quantum number (n) [1, 2, 3]. They tend to have exaggerated properties on account of their size. Some properties are stated in Fig. 1.1.

Due to the existence of large n states, interesting properties arise, for instance — when Rydberg atoms are placed in electric fields and demonstrate extreme sensitivity to it [4, 5], or when they are made to collide, ionize, or interact [6, 7, 8]. They also have relatively long radiative lifetime — typically of the order of 100 μs for n = 50 [9] — making them even more appealing.

1.1.1 Rydberg Blockade

The Rydberg atoms being neutral, predominantly interact via neutral forces like dipole-dipole interaction. Another implication of large n is the existence of large dipole moment (around 3000x the dipole moment of water) in these atoms and hence strong dipole-dipole interactions [1, 10]. Fig. 1.2 [11] compares the energy scale of Rydberg atoms to that of the ground-state atoms. It is seen that the Rydberg dipole-dipole interactions (or van der Waals interactions) are comparable to Coulomb interactions, and are 12 orders of magnitude higher than the ground-state dipole-dipole interactions (or van der Waals interactions).

Property	n dependence	Na(10d)
Binding energy	n^{-2}	0.14 eV
Energy between adjacent n states	n^{-3}	0.023 eV
Orbital radius	n^2	147 a_0
Geometric cross-section	n^4	68 000 a_0^2
Dipole moment $\langle nd \vert er \vert nf \rangle$	n^2	143 ea_0
Polarizability	n^7	0.21 MHz cm^2/V^2
Radiative lifetime	n^3	1.0 μs
Fine-structure interval	n^{-3}	-92 MHz

Fig. 1.1: Scaling Properties of Rydberg atoms. Source: Table 2.4 from T. F. Gallagher, *Rydberg Atoms*, Cambridge Monographs on Atomic, Molecular and Chemical Physics, 3, pp 25, 1994. Copyright (1994) by the Cambridge University Press. Reprinted by permission.

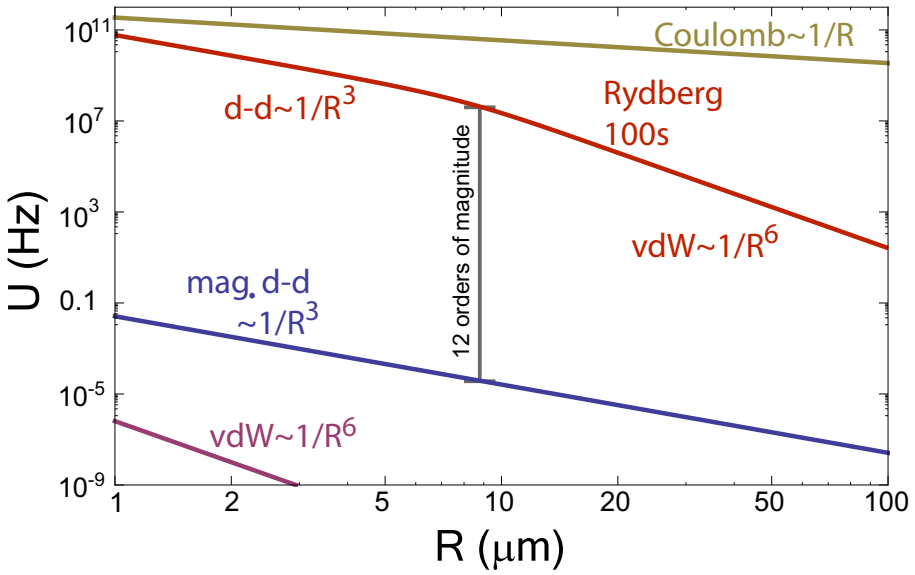

Fig. 1.2: Energy scale of Rydberg atoms compared to ground-state atoms. Reprinted figure with permission from M. Saffman, T. G. Walker, and K. Mølmer, Reviews of Modern Physics, 82(3), 2313, 2010. Copyright (2010) by the American Physical Society.

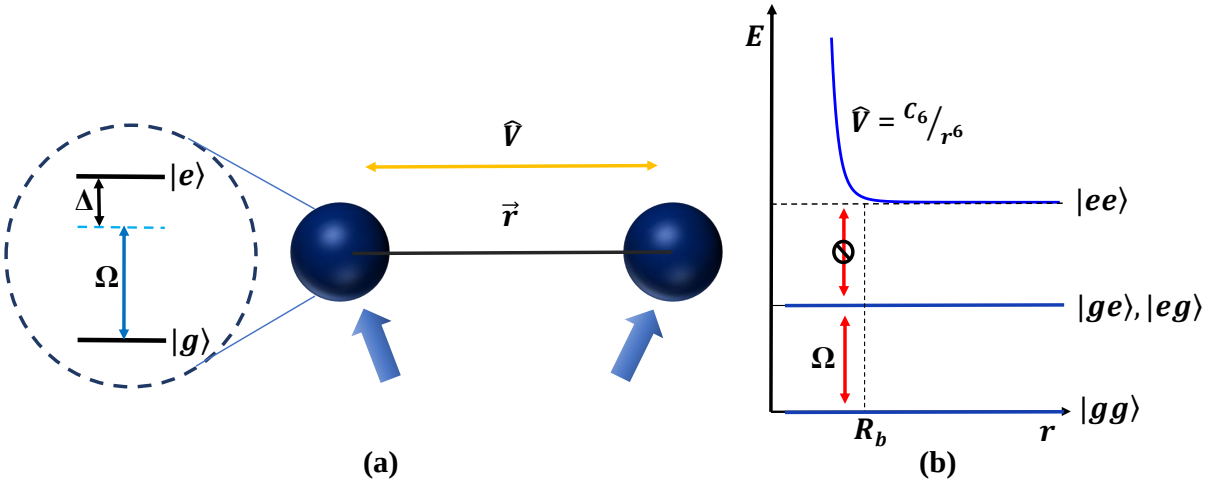

Fig. 1.3: Rydberg-Rydberg interactions ($\hat{V}$) between two two-level atoms at a separation r (a) System and the level scheme of the atoms being studied (b) Energy level diagram of the two interacting atoms. The dotted line shows the energy level in the absence of interaction, and the blue line shows the energy level in the presence of interaction. The state $|ee\rangle$ diverges at small separation, showing Rydberg Blockade.

To understand more of this interaction, consider two atoms — atom 1 and atom 2 separated by a distance r (much larger than the atomic size), as shown in Fig. 1.3(a).

The interaction between them is defined as —

$$\hat{V} = \frac{1}{4\pi\varepsilon_0 r^3}(\hat{d_1}\cdot\hat{d_2} - 3(\hat{d_1}\cdot\hat{\mathbf{r}})(\hat{d_2}\cdot\hat{\mathbf{r}})) \tag{1.1}$$

where $\hat{\mathbf{r}}$ is $\frac{\mathbf{r}}{r}$, unit vector of separation between atoms, and $\hat{d_i}$ is the dipole moment of atom i.

For large separations, away from Förster resonances, this interaction is in the van der Waals regime where interaction is of the form $\frac{C_6}{r^6}$ ($C_6 \propto n^{11}$). For shorter separations, the interaction is in the strong dipole regime and is of the type $\frac{C_3}{r^3}$ ($C_3 \propto n^4$). A very interesting observation of this is dipole blockade, which is shown in Fig. 1.3(b). Dipole blockade is defined as the suppression of multiple excitations, hence allowing only single excitation in a radius (called blockade radius) around a Rydberg state owing to the strong interactions [12, 13]. This is due to interaction induced additional detuning for multiple excitation state and hence forbidding the transition to this state and suppressing its population.

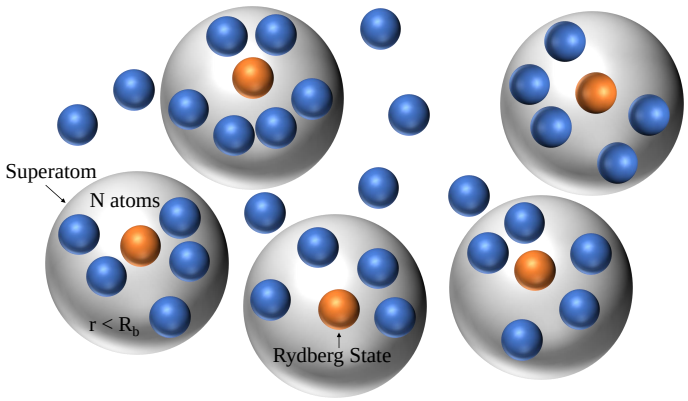

Fig. 1.4: Superatom: N atoms cluster within blockade radius (R_b) showing collective behavior.

An ensemble of N atoms within this blockade radius, referred as superatom (Fig. 1.4), forms two states: the ground-state $|g,g,g,....g,g\rangle$ and collective excited state $\frac{\Sigma_i|g,g,..e_i,..gg\rangle}{\sqrt{N}}$. The Rabi frequency of the ensemble is collectively enhanced by a factor of $\sqrt{N}$ [14], i.e. $\Omega_{Superatom} = \sqrt{N}\Omega_{Atom}$. Fig. 1.5 demonstrates collective excitation dynamics of one atom and four atoms (in the presence of strong interaction) showing enhancement of Rabi frequency. In the Fourier transform of the population dynamics, the peak for N=4 is at a frequency twice that for N=1.

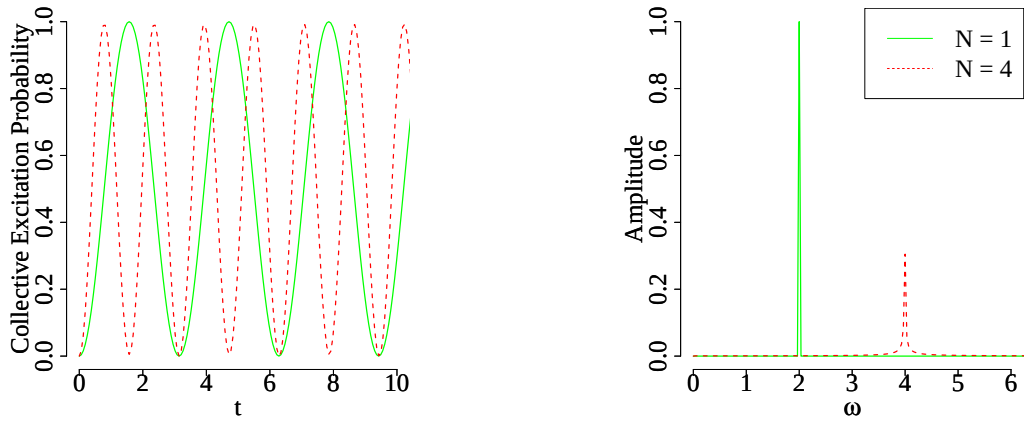

(a) Excitation dynamics showing the enhancement of Rabi frequency

(b) Fourier Transform of Excitation dynamics

Fig. 1.5: Collective enhancement of Rabi frequency for $\Omega = 1$ and $\Delta = 0$ (a) Single excitation dynamics (<P_e>) for the two systems, showing an enhancement in the frequency of oscillation. (b) Fourier Transform of the single excitation dynamics.

1.1.2 Recent Developments in this field

Theoretical Developments — Rydberg atoms are becoming a popular system for exploring novel properties, providing a wide scope for research. Their dynamics have been used to uncover the connection between stationary quantum wave functions and classical orbiting dynamics of electron wave-packets [15, 16, 17]. Quantum non-demolition photon state measurements are allowed, using Rydberg atoms in high-Q resonant cavity [18, 19].

It is known that ultracold-atomic systems are used as models for quantum many-body systems that have applications in condensed matter physics. Rydberg atoms, due to their strong and long-range interactions, are potential candidates for the replacement of models implementing the previously analyzed ground-state atoms. They are used to implement interacting spin models, for example — the xy model [20, 21, 22].

Recently, formation of exotic molecular states are seen due to the coupling between two Rydberg atoms or between a Rydberg atom and a ground-state atom [23, 24, 25, 26]. The strong Rydberg interactions make them suitable for quantum simulation of spin model [27] or in the implementation of two-qubit entangled quantum gates [28]. Along with strong interactions, dissipation could lead to exotic phases in ultracold many-body atomic systems, "such as uniform phase, antiferromagetic phase, oscillatory phase, and even the bistability between these phases" [29, 30, 31]. Their high polarizability gives rise to non-linear optics [32].

Experimental Developments — On the experimental avenue, the research on Rydberg atoms is limited due to their strong interactions and limited lifetime. Recently evidence of the blockade has been observed in Rydberg excitation in large samples [33, 34]. There have been observations of blockade having applications in quantum phase gates [10, 35].

A much more recent observation is antiblockade [36, 37], which is a result of three-level systems and their interaction with light. Strong Rydberg–Rydberg interactions lead to non-linear optics, such as slow propagation of pulse in an electromagnetically induced transparency setup [38] and photon-photon interactions induced blockade [39, 40].

With the recent work [41] done by physicists at the University of Innsbruck, a first move towards quantum simulation of high energy theory using atomic physics is established, bridging ultracold physics and high-energy physics. The importance of gauge theories is invaluable in studying interactions between fundamental particles, but it has always been a challenge computationally. Schwinger model — quantum electrodynamics in 1D — is used to test gauge theories as it shares similarities with quantum chromodynamics. Using trapped ions, by mapping fermionic operators to spin operators using Jordan–Wigner transformation, the real-time evolution of Schwinger model is studied. The instability that arises due to quantum fluctuations can manifest as creation of electron-positron pair. With this paper, a future for quantum simulation of non-abelian gauge theories can be seen.

1.1.3 Rydberg Dressing

As mentioned, Rydberg atoms provide great scope for research, but there might arise issues regarding the limited lifetime of Rydberg atoms or with controlling the strong interactions of Rydberg atoms. One method to address these issues is Rydberg dressing. Ground-state atoms have a long lifetime but the interaction between them is weak, whereas Rydberg atoms have a limited lifetime but strong interactions. Rydberg-dressed systems have the best of both worlds. Their long range interaction and large life expectancy make them a promising candidate to study many-body physics. Rydberg dressing has emerged as an exciting and valuable tool when studying Rydberg interactions. Rydberg dressing can be simply put as dressing of laser fields to strongly interacting Rydberg states, where the result will be maximum population in the ground-state with a few existing in the Rydberg state [42].

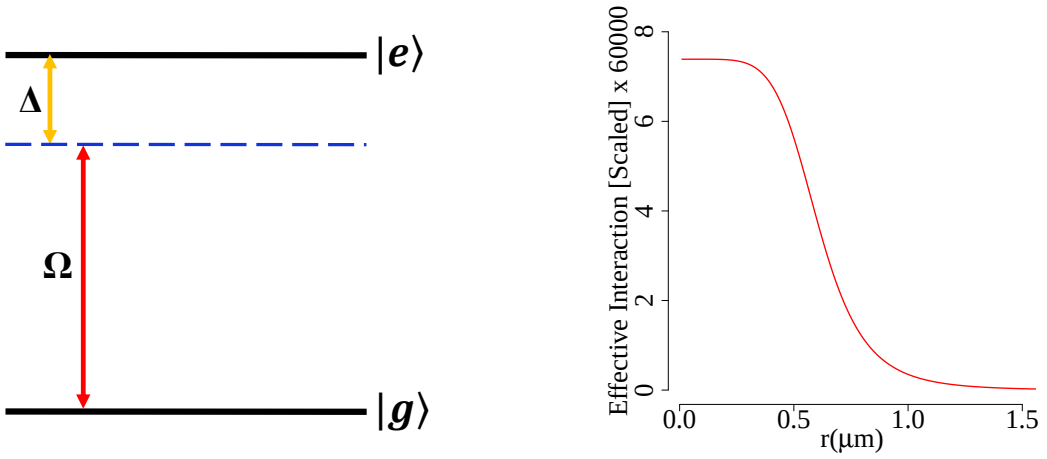

Fig. 1.6: (a) Dressed Two-level System (b) Soft-Core Potential attained for $\Delta = 10\Omega$ and $\Omega = 1$. The effective interaction is scaled using Rabi frequency.

For a single atom having ground-state $|g\rangle$ and excited state $|e\rangle$, a dressed state is defined as $|Dressed\rangle = |g\rangle - \frac{\Omega}{2\Delta}|e\rangle$. As the parameter $\frac{\Omega}{2\Delta}$ is changed, the extent of the excited state present in the dressed state changes. Generally, it is kept as small as 0.1, to ensure a long lifetime and controllable interaction. For a small parameter value, the effective interaction ($U(r)$) between two such dressed atoms forms a soft-core potential as in Fig. 1.6. An example of Rydberg dressing is ultracold gases being weakly dressed with Rydberg atoms to control the type and strength of the inter-atomic interactions present in the gas [9]. Based on this, some exciting opportunities have been proposed; for instance, the calculation of Hubbard parameters of Rydberg dressed atoms [43]. "Contrary to dipolar gases, where the interactions follow an inverse cubic law, the key feature of Rydberg-dressed interactions is the possibility of making neighboring couplings to the same magnitude as that of the on-site ones in optical lattices" [43]. This has a tremendous advantage in that one need not consider extra parameters to define neighboring site interactions in the model. Recent experimental realization of Rydberg dressing provides a good support for the aforementioned properties [44, 45].

1.2 Project Development

This thesis studies in detail dissipative dynamics in ultracold Rydberg atomic setups including two-level and multi-level schemes. In particular, for the latter case, we focus on the electromagnetically induced transparency (EIT) based setups. In the dilute gas limit, away from the Förster resonances, the interactions are of van der Waals's type with anisotropic character depending on the angular states. For the dissipative systems, studies are done in the density picture using the master equation for density matrix, whereas for the non-dissipative systems, a simple time-dependent Schrödinger equation is used. To begin with, in this project we analyzed in detail the recent proposal for generating Rydberg-dressed interactions, based on a scheme with electromagnetically induced transparency, utilizing metastable states of alkaline earth atoms [46]. These Rydberg-dressed interactions lead to exotic curves of effective interaction for different separations, showing presence of a maximum at a finite separation. We studied and understood this exotic nature and extended it to different systems. As these results were attained for steady state, the time evolution of such systems was subsequently studied. Furthermore, the analyses of effective interactions were extended to different novel systems and the time dynamics was analyzed for different level schemes and unique systems. The expected results of the time dynamics analysis were the famous Rabi oscillations. However, extensions to new systems resulted in exciting unique dynamics. The physics dealt with in this project is mostly limited to few body interactions. The novel properties of Rydberg atoms arise from the strong interactions in many-body physics, which lead to unique properties due to collective behavior. Therefore, for an insightful analysis, while exploring the dynamics of the two-level scheme, we extended the system to a many-body system — with the reproduction of results [21, 47] for the classical field and then an extended analysis in the presence of a quantized field — Fock state and coherent field state.

1.3 Overview

In Chapter 1, we developed motivation behind this thesis and the need to understand Rydberg atoms and their the possible applications. Basics of Rydberg atoms — properties, interaction, blockade, and dressing were discussed. Finally, an outline of our project was developed.

In Chapter 2, standard systems that we planned to extend were analyzed, by reproducing existing results and plots of these systems. We also reviewed the literature behind these results and developed theory in the direction of our extensions.

Chapter 3 summarizes the observations and results of our investigations. These are discussed in detail and their implications are analyzed.

Chapter 4 concludes this thesis with a summary of the work and briefly indicates the directions that can be explored in the future as an extension of the work that forms the body of this thesis.

2

Theory

As the project deals with different systems, for simplicity it is broadly classified on the basis of level schemes — Two-level, Three-level, and Four-level. The two-level scheme is well explored; such as analyzing excitation dynamics for non-interacting atoms or studying effective interactions between interacting Rydberg atoms.One motivation for pursuing this scheme, even though it is studied thoroughly, is that it will act as a stepping stone to three-level and four-level schemes. In addition to that, there are still some unexplored dynamics in two-level systems; such as dissipative excitation dynamics with classical field for interacting atoms, or even simple excitation dynamics with quantized field for interacting atoms (extension of Jaynes–Cummings Model). This chapter is divided on the basis of the classification introduced above, so as to prioritize different systems for each level scheme.

Contents

2.1 Two-Level scheme

Shown in Fig. 2.1, a two-level atom has two energy states, ground-state $|g\rangle$ and the excited state $|e\rangle$. The energy of the ground-state is $\hbar\omega_g$ and the energy of the excited state is $\hbar\omega_e$.

Therefore, the atomic Hamiltonian ($\mathscr{H}_A$) can be described as —

$$\mathscr{H}_A = \hbar\omega_g |g\rangle\langle g| + \hbar\omega_e |e\rangle\langle e| \tag{2.1}$$

The transition energy from $|g\rangle$ to $|e\rangle$ is defined as $\hbar\omega_{ge}$.

We study the atoms' interaction with classical and quantized field. First, we focus on the classical field, as much is explored here, and then we extend our analysis to quantized field.

2.1.1 Atom interacting with Classical Field

The atom is placed in a classical electromagnetic field with frequency ω. The interaction between the field and atom is given by —

$$\mathscr{V}^{AF} = -\mu \cdot \mathbf{E}(t) = \mu E(t) \tag{2.2}$$

where μ is the dipole operator, and $\mathbf{E}(t)$ is the electromagnetic field. Hence, the atom field Hamiltonian is defined as [48] —

$$\mathscr{H} = \mathscr{H}_A + \mathscr{V}^{AF} = \hbar\omega_g |g\rangle\langle g| + \hbar\omega_e |e\rangle\langle e| - \mu_{ge}\mathscr{E}e^{i\omega t} - \mu_{eg}\mathscr{E}*e^{-i\omega t} \tag{2.3}$$

Defining Ω as $-\dfrac{\mu_{ge}\mathscr{E}}{\hbar}$

$$\mathscr{H} = \hbar\omega_g |g\rangle\langle g| + \hbar\omega_e |e\rangle\langle e| + \hbar\Omega(e^{i\omega t} + e^{-i\omega t}) \tag{2.4}$$

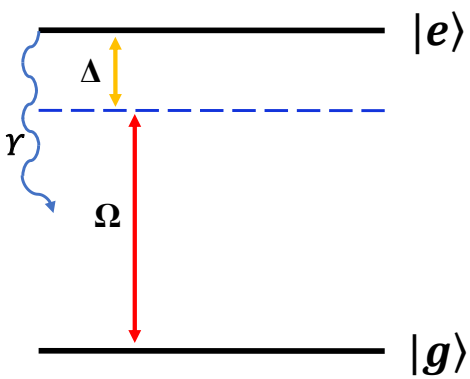

Fig. 2.1: Two-level atom with spontaneous emission rate γ placed in an electromagnetic field. Ω couples the two states, and is detuned by Δ.

The Hamiltonian after transformation [49] is written as —

$$\mathscr{H} = \frac{\Omega}{2}(|g\rangle\langle e| + |e\rangle\langle g|) + \Delta(|e\rangle\langle e|) \tag{2.5}$$

2.1.1.1 Non-Dissipative Dynamics ($\gamma = 0$)

The population of the states in the presence and absence of detuning show (in Fig. 2.2) the oscillatory behavior famously known as Rabi oscillations. The frequency of oscillation for resonant transition is known as the Rabi frequency (Ω), whereas for non-resonant transition it is the effective Rabi frequency ($\Omega_{eff} = \sqrt{\Omega^2 + \Delta^2}$).

The Rabi oscillations still exist if the numbers of atoms are increased, though the frequency of oscillation increases as the number of atoms increase, as population of n atom states P_n is P_1^n, where P_1 is the one atom population. To restate this, population of ground and excited states for two atoms are shown in Fig. 2.2, which establishes that increase in the number of atoms increases the frequency of oscillation.

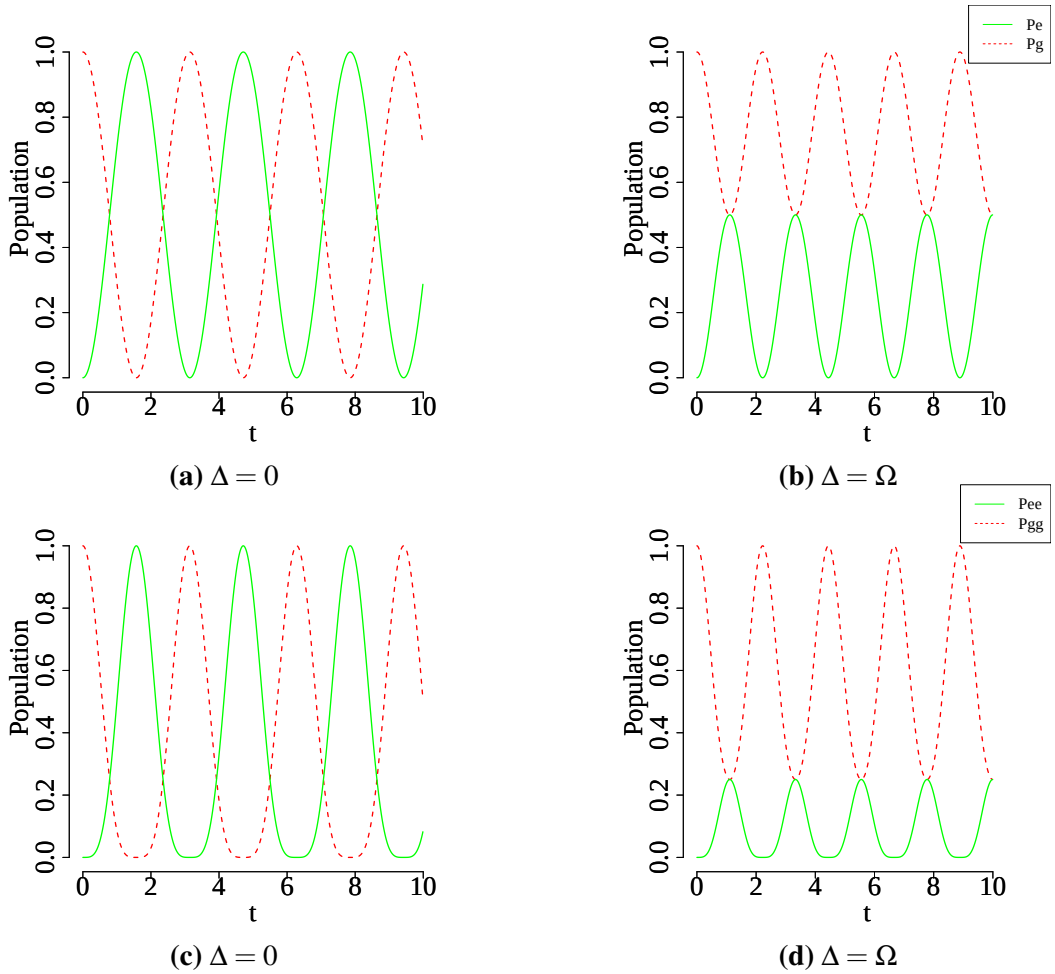

(a) $\Delta = 0$ **(b)** $\Delta = \Omega$

(c) $\Delta = 0$ **(d)** $\Delta = \Omega$

Fig. 2.2: Rabi oscillations for one atom (a and b) and two atoms (c and d) for $\Omega = 1$: ground-state population and excited state population.

2.1.1.2 Dissipative Dynamics ($\gamma \neq 0$) — Master Equation

To analyze dissipative atomic setups, the concept of density master equations is introduced. Time-dependent Schrödinger equation works well for non-dissipative dynamics, but in the presence of dissipation it fails. The density master equations are differential rate equations of density (ρ) matrix, given by [46] —

$$\partial_t \hat{\rho} = -i[\hat{\mathscr{H}}, \hat{\rho}] + \mathscr{L}(\hat{\rho}) \tag{2.6}$$

where, $\mathscr{L}(\hat{\rho})$ is the Lindblad operator —

$$\mathscr{L}(\rho) = C_e \hat{\rho} C_e^+ - \frac{1}{2}(C_e^+ C_e \hat{\rho} - \hat{\rho} C_e^+ C_e) \tag{2.7}$$

with, γ being the decay rate from an excited state $|e\rangle$ to a ground-state $|g\rangle$ as shown in Fig. 2.1.

$$C_e = \sqrt{\gamma} |g\rangle \langle e| \tag{2.8}$$

2.1.1.3 Dissipative Dynamics ($\gamma \neq 0$)— Results

The Rabi oscillations decay with the introduction of dissipation, as it can be seen in Fig. 2.3 for one atom —

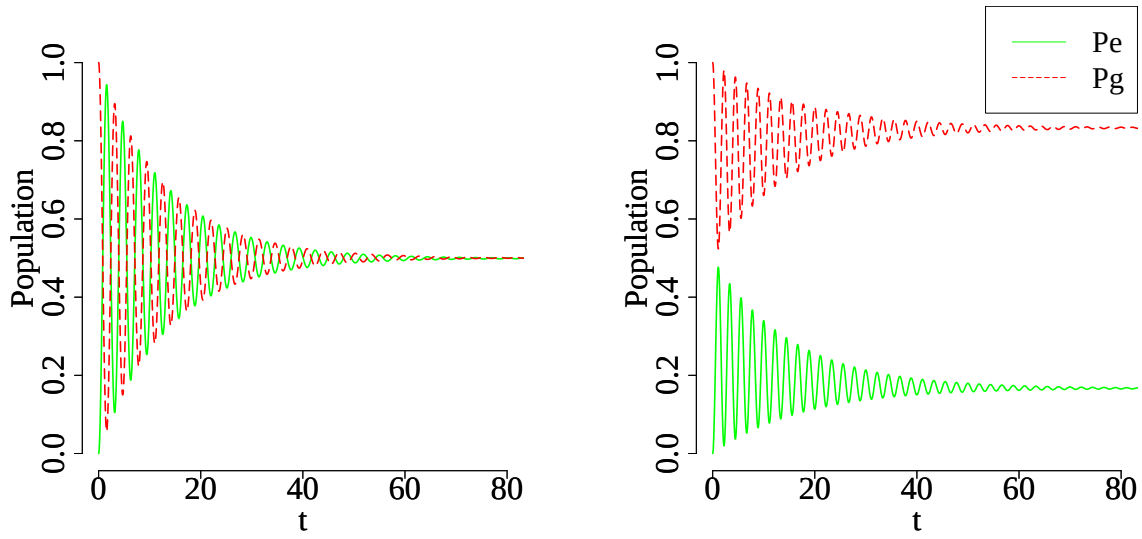

(a) $\Delta = 0$ **(b)** $\Delta = \Omega$

Fig. 2.3: Dissipative Oscillation of the ground-state (P_g) and the excited state (P_e), for one atom. $\Omega = 1$, $\gamma = 0.1$.

The states stop oscillating over time and decay to a steady state. The definition of this steady state only depends upon the Rabi frequency and the detuning, and is independent of the choice of the initial states.

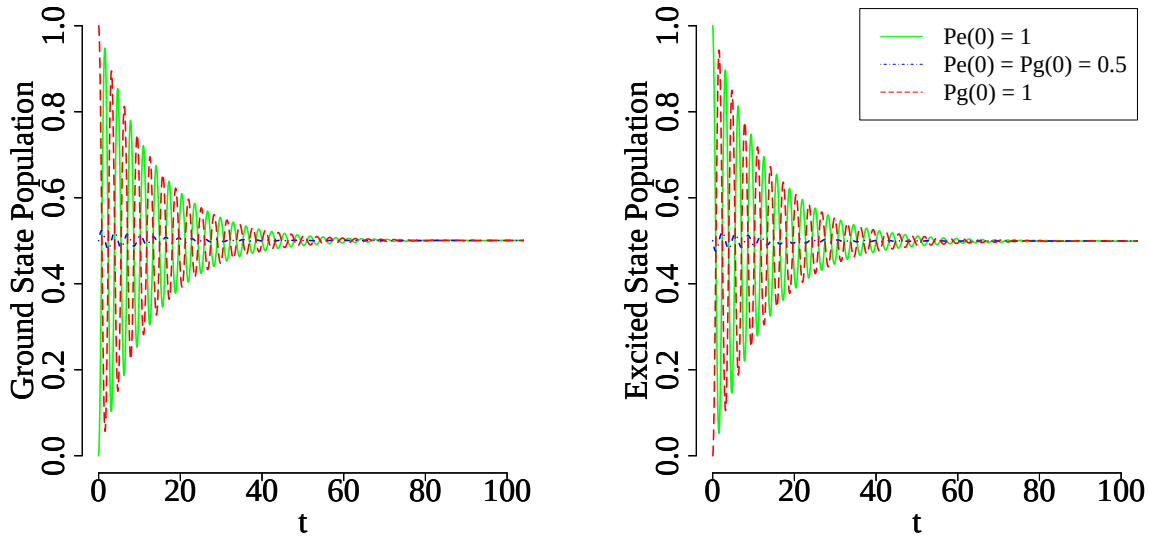

(a) Ground-state population (P_g) **(b)** Excited state population (P_e)

Fig. 2.4: Dissipative Resonant Oscillation of the two states for different initial conditions, keeping $\Omega = 1$, $\Delta = 0$, $\gamma = 0.1$. Different initial conditions result in the same steady state.

As the evaluation of the master equations is computationally inefficient, this system is only extended to two atoms to observe the dependence of Rabi oscillations on the number of atoms.

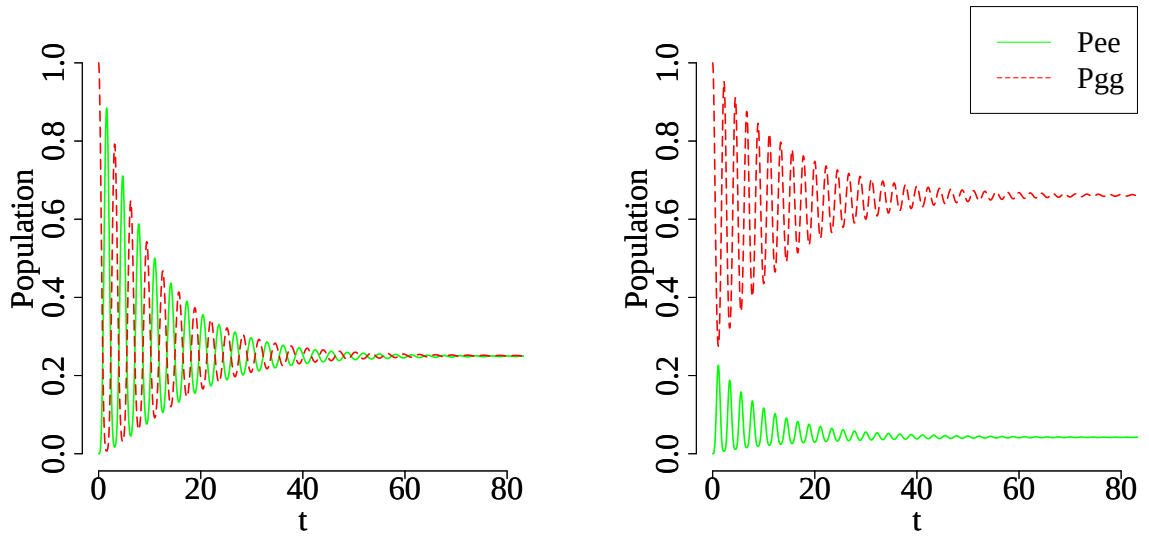

(a) $\Delta = 0$ **(b)** $\Delta = \Omega$

Fig. 2.5: Dissipative Oscillation of the ground-state (P_{gg}) and the excited state (P_{ee}), in the presence of detuning for two atoms. $\Omega = 1$, $\gamma = 0.1$.

With the increases in the number of atoms, the steady state is achieved faster. The definition of the steady state is still independent of the choice of the initial states and solely depends on the Rabi frequency and detuning.

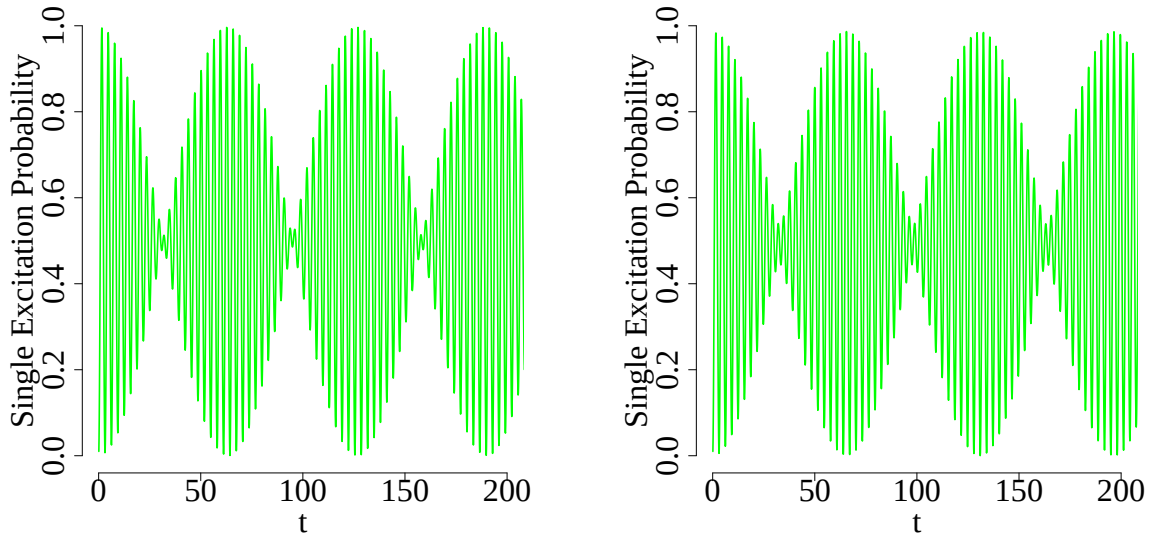

(a) $\Delta = 0$ **(b)** $\Delta = V/3$

Fig. 2.6: Single Excitation dynamics (<P_e>) for weak interaction strength between two atoms. The above analysis is done for $\Omega = 1$ and $V = 0.2\Omega$

2.1.1.4 Excitation Dynamics of Interacting Atom

In this section, a system of two atoms interacting with van der Waals interaction is studied. The van der Waals interaction is given by [49] —

$$\mathscr{W} = \frac{C_6}{r^6} |e\rangle \langle e| \otimes |e\rangle \langle e| \tag{2.9}$$

The excitation dynamics are studied for weak and strong interactions. Fig. 2.6 shows the single excitation dynamics for weak interaction (0.2Ω) with resonant and off-resonant transition. Fig. 2.6 shows per site excitation P_e for interaction strength 0.2Ω. The famous Rabi oscillation gets modified to form envelopes. In the presence and absence of detuning, the excitation dynamics do not change as the detuning provided is weak. The formation of envelopes is due to the addition of another frequency arising from the presence of interaction [49]. These plots also hint on the existence of collapse and revival of the excitation dynamics. We will see this becoming more pronounced for higher number of atoms.

Fig. 2.7 shows the single excitation dynamics in the presence of strong interaction (5Ω) for resonant and off-resonant transition. The envelopes disappear in the presence of strong interaction [49]. The presence of detuning, does not affect the trend, it simply suppresses the population.

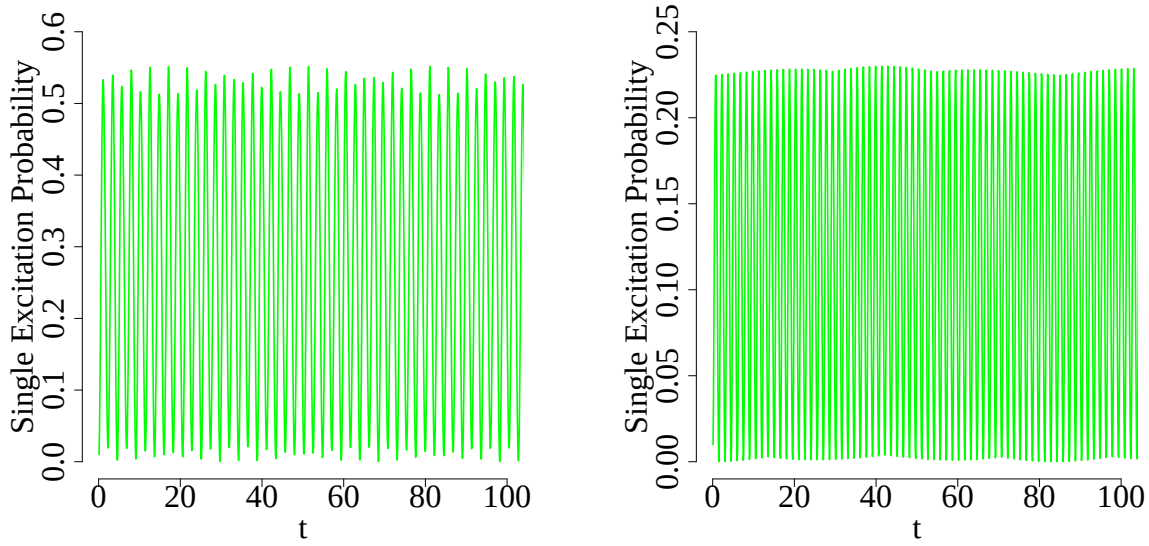

(a) $\Delta = 0$ **(b)** $\Delta = V/3$

Fig. 2.7: Single Excitation dynamics (<P_e>) for strong interaction strength between two atoms. The above analysis is done for Ω = 1 and V = 5Ω

2.1.1.5 Effective Interaction

The effective interaction ($U(r)$) is defined as the energy of the dressed state (defined in Section 1.1.3), but in the case of a non-dressed system, it is taken as the Hamiltonian ground-eigenstate energy. The higher the parameter, the stronger the effective interaction. The effective interactions in Fig. 2.8 show the famous soft-core potential.

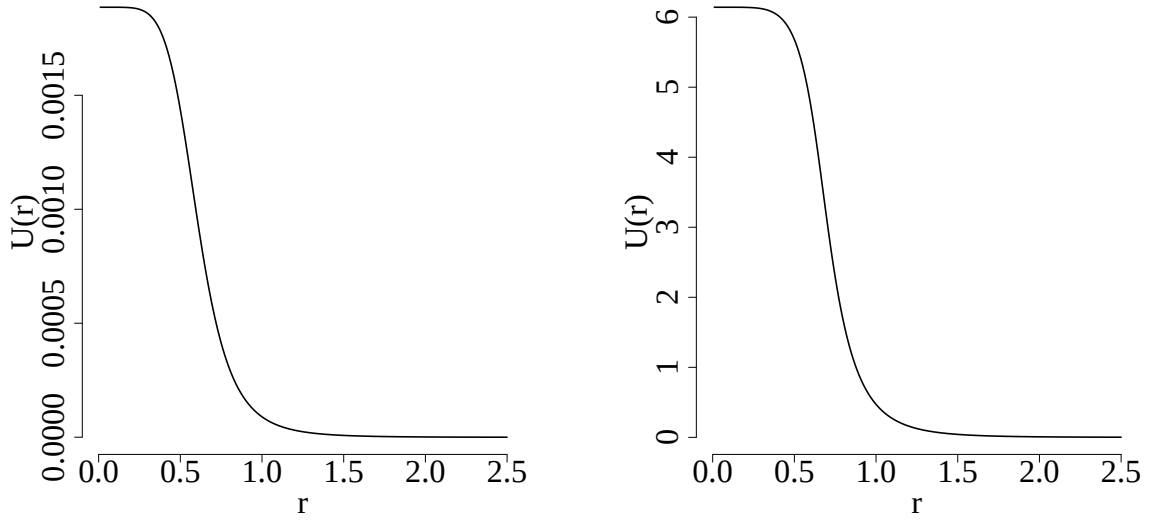

(a) $\Omega/\Delta = 0.2$ **(b)** $\Omega/\Delta = 5$

Fig. 2.8: Effective Interaction vs Separation for different dressing parameters. It is computed for Ω =1 and C_6 = Ω. The effective interaction is scaled using Rabi frequency Ω.

2.1.1.6 Two-Point Correlation function

The normalized two-body spatial correlation [50] is —

$$g^2(r) = \frac{G^2(r)}{\langle P(r_1)\rangle \langle P(r_2)\rangle} \tag{2.10}$$

where $G^2(r)$ is defined as $\langle \Psi^+(r_1)\Psi^+(r_2)\Psi(r_1)\Psi(r_2)\rangle$, the probability of detecting two particles simultaneously at r_1 and r_2 and $\langle P(r_1)\rangle$ and $\langle P(r_2)\rangle$ are probabilities of finding a particle at position at r_1 and r_2.

In the system of two interacting Rydberg atoms, the normalized two-body spatial correlation is the probability of both the particles being in the excited state at a separation of r [50] is —

$$g^2(r) = \frac{\langle P_{ee}(r)\rangle}{\langle P_e^1(r)\rangle \langle P_e^2(r)\rangle} \tag{2.11}$$

Here, two definitions of average are used, population at steady state and the time averaged population. Fig. 2.9 analyzes the two-point correlation function for population at steady state and time–averaged population, for two different transitions: resonant and detuned (non-resonant).

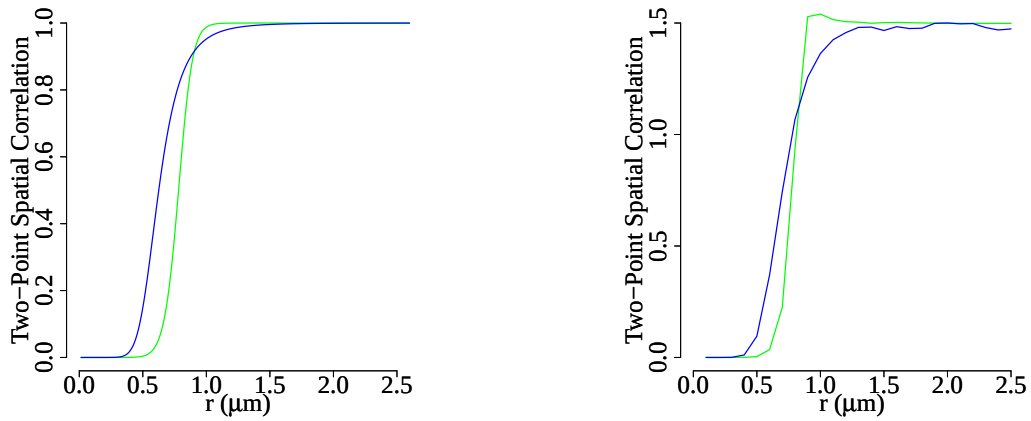

(a) Steady-State population **(b)** Time-averaged population

Fig. 2.9: Two-Point Spatial Correlation for two atoms, with different definition of average. Resonant case ($\Delta = 0$) in green. Non-resonant case ($\Delta = 10\Omega$) in blue.

The Rydberg blockade radius is less in the case of non-resonant transition, as the excited state population is suppressed due to detuning. In Fig. 2.9, the two definitions of the two point correlation function are also compared. Even though the physics attained from both the definitions is similar, there are differences. The time–averaged population shows the trend of sudden increase in the population and attaining maximum, just after the blockade radius. After the maximum, it oscillates and eventually converges to its far-separation population [51]. This trend is hidden in the steady state definition. The time averaged population also leads to an enhancement to 1.5, as the time averaged population for double excitation is not the same as the product of two time averaged population of single excitation for large separation.

2.1.2 Atom interacting with Quantized Field

Previously, all the studies were limited to a quantum system (atom) interacting with a classical field. In this part, the idea of a quantized field is introduced. The Hamiltonian of the quantized field containing a single mode [52] —

$$\mathscr{H}_F = \hbar\omega_f\left(a^+a + \frac{1}{2}\right) \tag{2.12}$$

where the field frequency is ω_f, a and a^+ are the annihilation and creation operators of the field. The quantized field is represented using a number state $|n\rangle$, where n is the number of photons.

2.1.2.1 Jaynes–Cummings Model

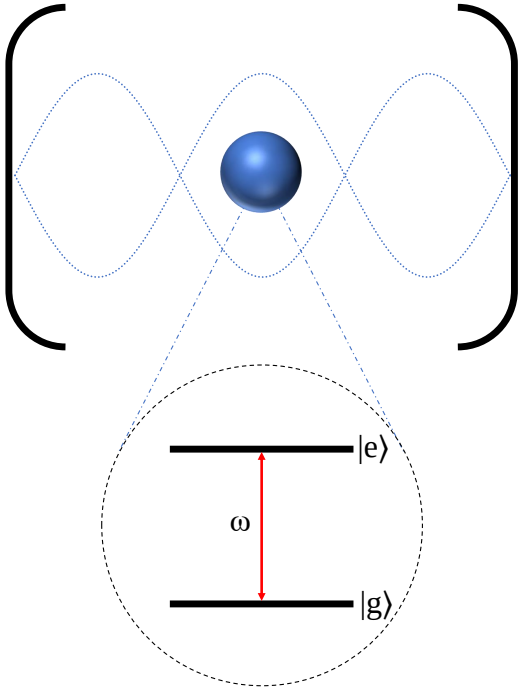

Fig. 2.10: Illustration of the Jaynes-Cummings model.

The simplest quantum model of the atom interacting with a quantized model is the Jaynes–Cummings Model which describes a two-level atom in a cavity interacting with a single mode quantized model. The system is described by Fig. 2.10. The atom has a two-level scheme, similar to the classical section with the frequency of transition being ω.

The Jaynes–Cummings Hamiltonian is [52] —

$$\mathscr{H} = \hbar\omega_f a^+a + \hbar\omega\,|e\rangle\langle e| + \hbar g(|e\rangle\langle g|\,a + |g\rangle\langle e|\,a^+) \tag{2.13}$$

where g is the atom-field coupling constant.

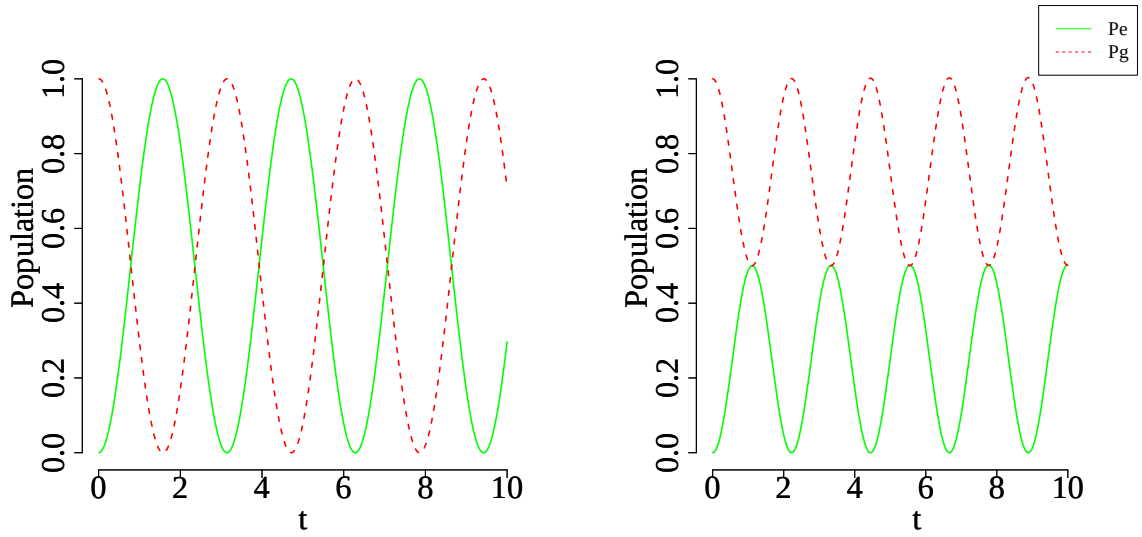

(a) $\Delta = 0$ **(b)** $\Delta = \Omega_n$

Fig. 2.11: Ground-state and Excited state Oscillations for one atom interacting with a quantized field (n=1) in the presence and absence of detuning.

Compared to the classical picture, the Rabi frequency is given as $2g$ for a single photon system.

The population shows Rabi oscillations in the presence and absence of detuning, as seen in Fig. 2.11. The trend is similar to the oscillations seen in the case of classical field.

The Rabi frequency for this system is defined as $\Omega_n = 2\sqrt{n+1}\mathrm{g}$. Hence, with the increase in the number of photons n, the frequency of oscillations increases. This is intuitive, as the number of photons in quantized field is equivalent to the intensity of the field in classical case.

2.1.2.2 Extension of JCM –Coherent Field State

So far, the field is taken to be a Fock state. In order to understand the collapse and revival behavior of Rabi oscillations, the initial field state is taken to be a coherent field state [52] —

$$|\alpha\rangle = \sum_{n=0}^{\infty} \frac{\alpha^n}{\sqrt{n!}} e^{-|\alpha^2|/2} |n\rangle \tag{2.14}$$

where $\alpha = \sqrt{\bar{n}}$, $\bar{n}$ being the mean number of photons.

This system is the epitome for studying and observing collapse and revival behavior, due to the perfect quantum field — coherent field. This field provides various number of photons, and for each photon number a Rabi frequency is defined. These Rabi frequencies interfere in a constructive and destructive manner to give rise to collapse and revival of oscillations [52].

The excitation dynamics for different mean photon numbers is shown in Fig. 2.12. By increasing the mean number of photons, the behavior becomes more defined and periodic.

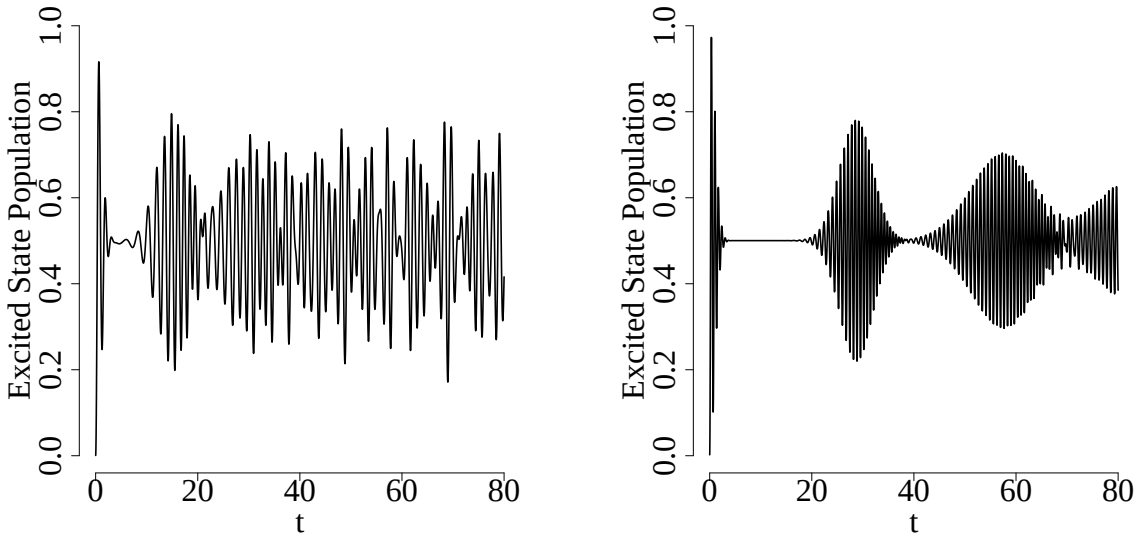

(a) $\overline{n} = 5$ **(b)** $\overline{n} = 20$

Fig. 2.12: Rabi Oscillation for one atom interacting with coherent field for different mean photon numbers.

2.2 Three-level interacting atoms

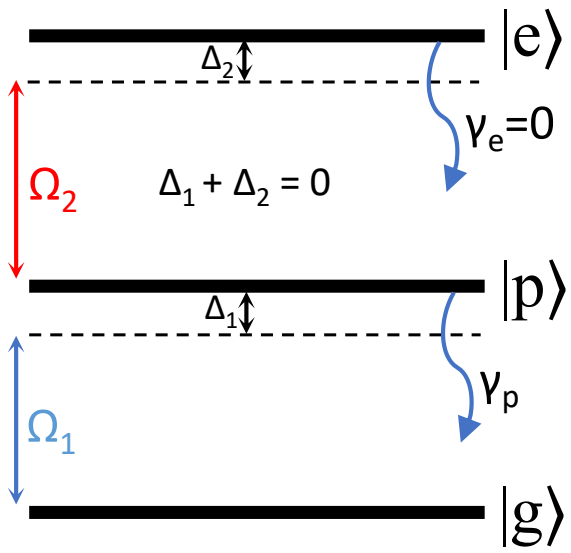

Fig. 2.13: System of Three level interacting atoms.

The three-level system is an exciting system. The three-level excitation dynamics is similar to two-level, hence the study of effective interaction is stressed upon in this section. All the studies are done assuming classical field. The system is described in Fig. 2.13.

Consider N such three-level atoms interacting via van der Waals interaction. The system is studied in electromagnetically induced transparency(EIT) setup [46].

One body Hamiltonian for the i^{th} atom is —

$$\mathscr{H}^i = \frac{\Omega_1^i}{2}(\hat{\sigma}_{gp}^{(i)} + \hat{\sigma}_{pg}^{(i)}) + \frac{\Omega_2^i}{2}(\hat{\sigma}_{ep}^{(i)} + \hat{\sigma}_{pe}^{(i)}) - \Delta_1 \hat{\sigma}_{pp}^{(i)} - (\Delta_1 + \Delta_2)\hat{\sigma}_{ee}^{(i)} \tag{2.15}$$

The interaction between the atoms i and j is —

$$\mathscr{W} = V(r_{ij})\hat{\sigma}_{ee}^{(i)}\hat{\sigma}_{ee}^{(j)} \qquad \text{where } V(r_{ij}) = C_6/r_{ij}^6 \tag{2.16}$$

The total effective interaction is defined as the energy of the dressed steady state or the dressed dark state(the state devoid of the decaying intermediate state) in the absence of interaction. It is attained analytically as —

$$U(r) - i\mathscr{T}(r) = \frac{\Omega_1^4 V}{\Omega_2^4} \frac{4\Delta_1^2 + \gamma^2 + 4(4\Delta_1^2 + \gamma^2 + \Omega_2^2)(\Delta_1 - i\gamma)\frac{V}{\Omega_2^2}}{[2\Delta_1 + (4\Delta_1^2 - \gamma^2 - \Omega_2^2)\frac{V}{\Omega_2^2}]^2 + \gamma^2(1 - \frac{4V\Delta_1}{\Omega_2^2})^2} \tag{2.17}$$

in the limit $\gamma_p << |\Delta_1|$, $\Omega_1 << \Omega_2$, $\Omega_1 << \gamma_p$.

Effective interaction vs separation between two atoms is shown in Fig. 2.14 for $\frac{\Delta_1}{\gamma_p} = 2.5$ and $\frac{\Omega_1}{\Omega_2} = 0.1$. Here, $\frac{\Omega_2}{2\Delta_1}$ acts as a control parameter in changing the shape of the potential. The exotic nature of the curves can be explained due to the maximum occurring for $\frac{\Omega_2}{2\Delta_1} = 1$ for small separation, due to interaction induced two-body resonance that enables the enhanced interactions.

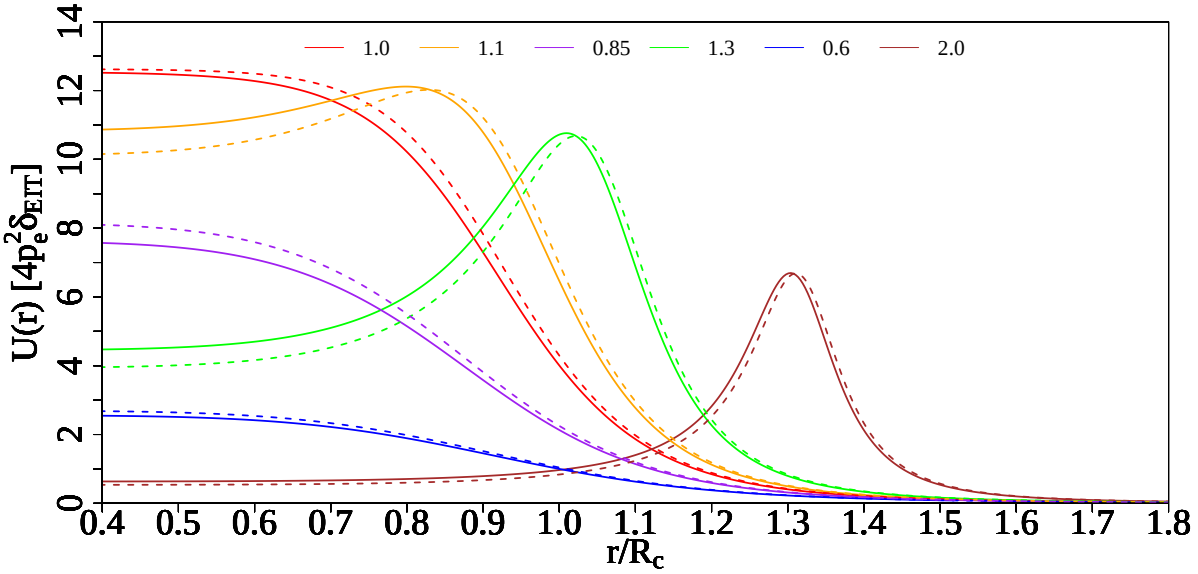

Fig. 2.14: Total Effective Interaction vs Separation for interacting three-level atoms in EIT setup based on the analysis in [46]. Control parameter $\frac{\Omega_2}{2\Delta_1}$ is varied; values in legend. Numerical solution in solid line and analytical solution in dashed line.

2.2.1 Three level interacting atoms — Method

In our project to analyze the three-level interaction, two-body density matrix master equations are used as a numerical tool. The two-body density master equations are given by [46] —

$$\partial_t \hat{\rho}_{ij}^{(2)} = -i[\hat{H}_i + \hat{H}_j, \hat{\rho}_{ij}^{(2)}] + \mathscr{L}_i(\hat{\rho}_{ij}^{(2)}) + \mathscr{L}_j(\hat{\rho}_{ij}^{(2)}) - i[\hat{W}_{ij}, \hat{\rho_{ij}^{(2)}}] - i\sum_{k\neq i,j} Tr_k[\hat{W}_{ik} + \hat{W}_{ik}, \hat{\rho}_{ijk}^{(3)}] \tag{2.18}$$

where, $\mathscr{L}_i(\hat{\rho}_i^{(1)})$ are the Lindblad operators and are given by —

$$\mathscr{L}[\rho] = \sum_m C_m \hat{\rho}_i^{(1)} C_m^+ + -1/2 \sum_m (C_m^+ C_m \hat{\rho}_i^{(1)} - \hat{\rho}_i^{(1)} C_m^+ C_m) \tag{2.19}$$

$$C_p = \sqrt{\gamma_p}\,|g\rangle\langle p|\,, C_e = \sqrt{\gamma_e}\,|p\rangle\langle e| \tag{2.20}$$

The total effective interaction is given by —

$$U(r) = Tr[\hat{\rho}_{12}^{(2)} H] \tag{2.21}$$

2.2.2 Extension of three-level interactions — Angular Dependence of C_6

For the three-level interacting system, the van der Waals interactions are taken to be isotropic — only dependent on the principal quantum number, as these are for Rydberg states of the form *ns*. As an extension to the three-level interacting dynamics, the effect of angular dependence is studied. For the same, the Rydberg states are taken to be of the form *np*.

van der Waals interaction between *ns* states is given by [53] as —

$$\mathscr{W} = \frac{(ea_0)^4 n^{11}}{r^6} \tag{2.22}$$

np states are not radially symmetric and are given by [53] as —

$$|r_0\rangle = \left|n^2 P_{3/2}, m = 3/2\right\rangle_z \text{ and} \tag{2.23}$$

$$|r_1\rangle = \left|n^2 P_{3/2}, m = 3/2\right\rangle_x \tag{2.24}$$

van der Waals's interaction between *np* states is given by [53] as —

$$\mathscr{W} = V_{00} = \frac{(ea_0)^4 n^{11} \sin^4(\theta)}{r^6} \tag{2.25}$$

$$\mathscr{W} = V_{11} = \frac{(ea_0)^4 n^{11} \cos^4(\theta)}{r^6} \tag{2.26}$$

2.2.3 Extension of three-level interacting atoms — 3-body Interaction

As a precursor to studying the effect of interaction in many-body systems, three-body interactions are studied and their relevance is studied. To do so, the three-body interaction are defined.

The three body interaction between them is given by [54] as —

$$\mathscr{W}_{ijk} = \frac{C_9(1+3(\cos(\theta)^3))}{r^9}\hat{\sigma}^1_{ee}\otimes\hat{\sigma}^2_{ee}\otimes\hat{\sigma}^3_{ee} \tag{2.27}$$

where $C_9 \approx \sqrt{C_6^3}$.

The total Hamiltonian for such systems (assuming three atoms) is given as —

$$\mathscr{H} = \mathscr{H}^1 + \mathscr{H}^2 + \mathscr{H}^3 + \mathscr{W}_{12} + \mathscr{W}_{23} + \mathscr{W}_{13} + \mathscr{W}_{123} \tag{2.28}$$

where, $\mathscr{H}^1$, $\mathscr{H}^2$ and $\mathscr{H}^3$ are the atomic Hamiltonian, $\mathscr{W}_{12}$, $\mathscr{W}_{23}$ and $\mathscr{W}_{13}$ are the two-body interactions, and finally $\mathscr{W}_{123}$ is the three-body interaction.

§

In this chapter, we revised the well-studied systems while exploring two-level and three-level schemes. In the two-level scheme, we studied the atom-light Hamiltonian for a classical field and a quantized field. For atoms interacting with a classical field, we analyzed the dynamics in the presence and absence of dissipation and interaction. Dissipation-less dynamics showed the famous Rabi oscillations, whereas the presence of dissipation decays the dynamics to a steady state defined by the detuning and the Rabi frequency. The dynamics gets modified in the presence of weak interaction to produce envelopes. In the strong interaction regime, the envelopes disappear and we see a suppression of the excited state population. In the presence of a quantized field, we study the Jaynes-Cummings model and its extension to coherent field state and observe the collapse and revival of the Rabi oscillation. We also briefly study the effective interaction and the two-point correlation function. The effective interaction takes up a soft core potential for a dressed state. In the three-level scheme we analyze the effective interaction to see the presence of exotic curves and extend this analysis to anisotropic interaction.

3

Results and Discussion

In this chapter, we extend the systems introduced in the previous chapter, attain new physics and suggest possible implications. Like the previous chapter, this chapter is broadly divided on the basis of level scheme. We start with the two-level scheme, where the classical dynamics studied till now is extended to time-dependent detuning and time-dependent Rabi frequency. These are examined for non-interacting atoms and dissipative excitation dynamics for interacting atoms in the few-body picture and interesting excitation dynamics and effective interaction in the presence of weak interaction in the many-body picture. Furthermore, we extend our analysis of two-level atoms in a classical field to a quantized field. After thoroughly studying the two-level scheme, we explore the three-level scheme. It is seen that the excitation dynamics attained for the three-level scheme is similar to that of the two-level scheme, but interesting results are attained when the effective interaction is studied. We extend this analysis of effective interaction to include angular dependence and three-body interactions. Finally, we extend the three-level system to a four-level system, where we study the effective interaction.

Contents

3.1 Two-Level Scheme

3.1.1 Atoms in Classical Field

In the previous section, we have understood the classical excitation dynamics for resonant and non-resonant transitions, and in dissipative and non-dissipative setups. Considering this area of research has been studied thoroughly, it is a surprise that there are still some exciting novel physics like excitation dynamics for many-body systems or even effective interaction for many-body systems. We mainly aim at analyzing many-body systems and finally extending our analysis of classical field to quantized field. We take our first step by analyzing two atoms and understanding the few body physics. It is seen previously that two parameters that play a key role in deciding the amplitude and frequency of oscillation and in the definition of the steady state are the Rabi frequency and the detuning. Hence, as a first step, we extend the current definitions of these key parameters in the hope of attaining novel dynamics.

3.1.1.1 Extension to Time dependent Detuning

In this section, a time-dependent detuning is considered. The detuning is defined as —

$$\Delta(t) = \Delta_0(1 + 2\alpha\cos(2\omega t)) \tag{3.1}$$

where α is kept small enough.

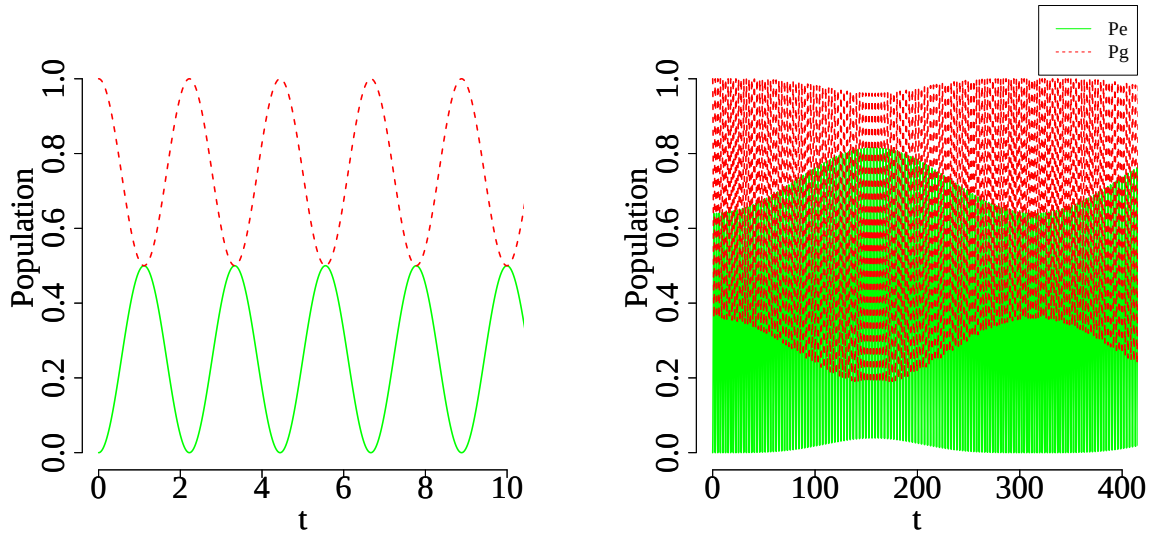

(a) $\Delta = 1$ **(b)** $\Delta(t) = 0.5(1 + 2(1/4)\cos((2)(0.01)t))$

Fig. 3.1: Comparison of Ground-state and Excited state dynamics for constant detuning and time-dependent detuning, keeping Rabi frequency Ω =1. The time-dependent detuning shows the formation of envelopes arising from the time-dependent amplitude of the state dynamics.

Fig. 3.1 compares the two systems, one with the constant detuning and the other with the time-dependent detuning. It was understood in the previous section, and can even be seen in Fig. 3.1 for constant detuning, the amplitude of the oscillations gets altered. This is because the detuning suppresses the transition to the excited state. Therefore, the oscillation of the ground-state range decreases (from [0,1] to [0.5,1] for $\Delta = \Omega$) and similar behavior is observed for the excited state. While analyzing the time-dependent detuning, it can be understood that the effect of the time-dependence appears on the amplitude of the oscillations. The amplitudes show an oscillating nature. The next step is to vary the different parameters in the equation and study how the dynamics of the states change.

Fig. 3.2 shows the Rabi oscillation attained by varying the different parameters in the equation. The first parameter considered is α, which decides the range of the variation of $\Delta(t)$. For instance, for α as $1/4$, Δ(t) varies from $\Delta_0(3/2)$ to $\Delta_0(1/2)$, whereas for α as $1/8$, Δ(t) varies from $\Delta_0(5/4)$ to $\Delta_0(3/4)$. Hence, the oscillation of Δ(t) gets altered in time and so does the oscillation of amplitude. Fig. 3.2(a) reassures this; with the decrease in α, the oscillation in amplitude decreases. The second parameter is Δ_0, which not only affects the range of the variation of Δ(t), it also alters the overall detuning. As evident in Fig. 3.2(b), with increase of Δ_0, not just the extent of amplitude oscillation increases, the suppression of the excited state population increases as well. Finally, the third parameter ω simply varies the period of the oscillation. As seen in Fig. 3.2(c), the increase in the value of this parameter increases the frequency of the amplitude oscillation, but the extent of the amplitude oscillation remains the same.

In Figs. 3.1 and 3.2, we see how time-dependence affects the period and amplitude of the oscillations. Our analyses thus far are for non-dissipative systems, where the effect of time-dependent detuning is seen on frequency and amplitude of Rabi oscillations. However, detuning also plays a key role in defining the steady state, necessitating the analysis of dissipative dynamics. With the tool of master equations, we extend the analysis to dissipative systems.

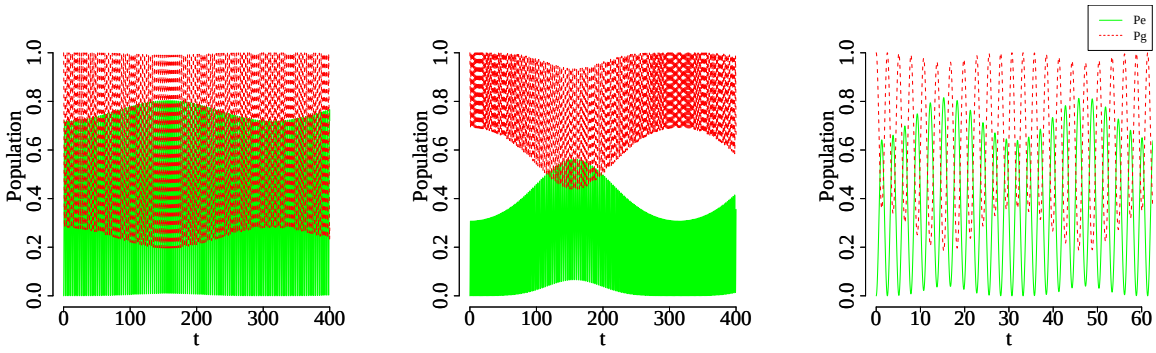

(a) α varied **(b)** Δ_0 varied **(c)** ω varied

Fig. 3.2: Ground-state and Excited state dynamics are shown for different parameters. The different definitions of the detuning are (a) $\Delta(t) = 0.5(1+2(1/8)\cos((2)(0.01)t))$, (b) $\Delta(t) = 1.0(1+2(1/4)\cos((2)(0.01)t))$ and (c) $\Delta(t) = 0.5(1+2(1/4)\cos((2)(0.1)t))$. Value of Rabi frequency Ω is kept as 1.

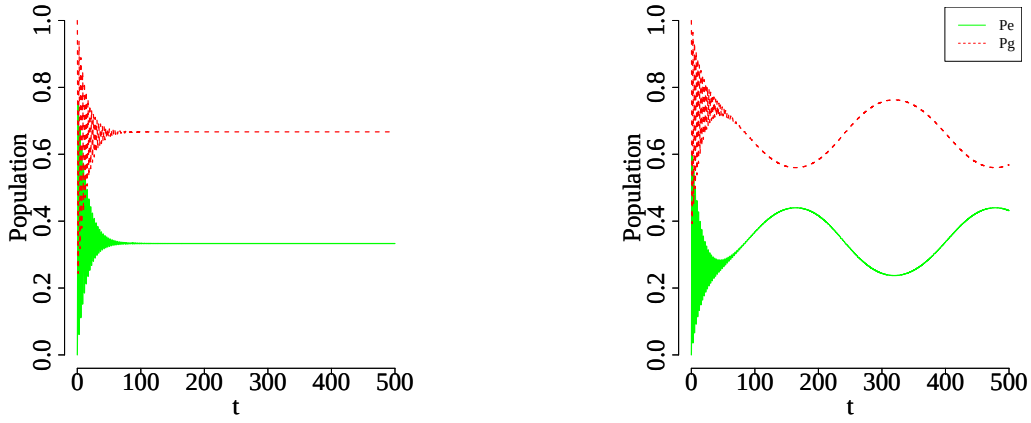

(a) $\Delta = 0.5\Omega$ **(b)** $\Delta(t) = 0.5(1+2(1/4)\cos((2)(0.01)t))$

Fig. 3.3: Comparison of dissipative ground-state and excited state dynamics for constant detuning and time-dependent detuning, keeping Rabi frequency Ω = 1 and decay rate $\gamma = 0.1\Omega$. The steady state attained for time-dependent detuning oscillates in time

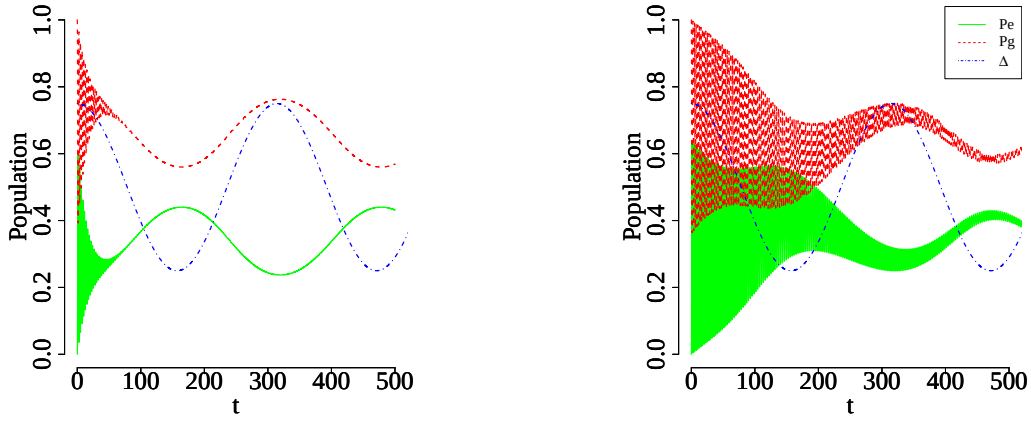

(a) $\gamma = 0.1\Omega$ **(b)** $\gamma = 0.01\Omega$

Fig. 3.4: Comparison of dissipative ground-state and excited state dynamics with time-dependent detuning for decay rates 0.1 Ω and 0.01 Ω. Detuning: $\Delta(t) = 0.5(1 + 2(1/4)\cos((2)(0.01)t))$ and Rabi frequency: Ω = 1. With two state dynamics, even time-dependent detuning is shown. Dynamics of the steady state is similar to that with detuning.

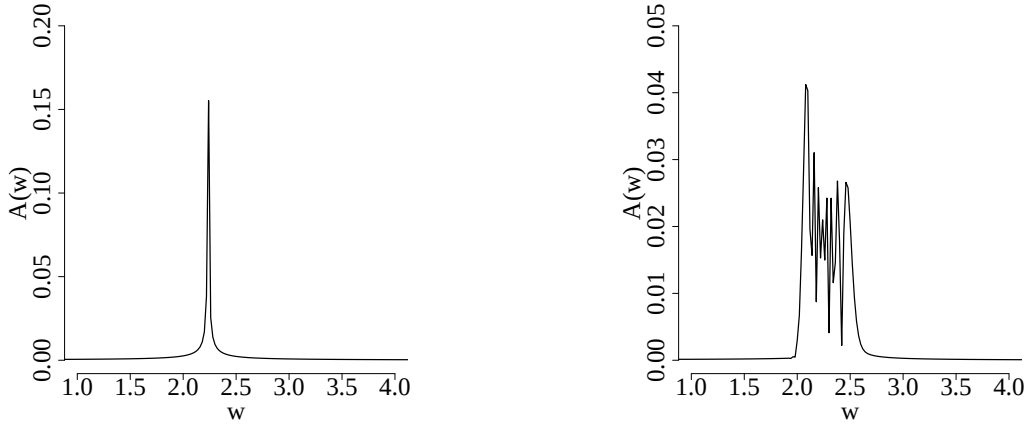

(a) $\Delta(t) = 0.5$ **(b)** $\Delta(t) = 0.5(1+2(1/4)\cos((2)(0.01)t))$

Fig. 3.5: Fourier Analysis of Constant detuning and time-dependent detuning for Rabi frequency Ω = 1. The presence of multiple peaks are seen in the Fourier analysis of time-dependent detuning

Fig. 3.3 compares the steady state in the presence and absence of the time-dependence of detuning. With a constant detuning, the steady state is defined as the state to which the oscillating states collapse to. For a two-level atom interacting with light, the steady state is the ground dressed state which is constant in time. Once the detuning is time-dependent, the ground dressed state starts oscillating with time. Hence, the steady state no longer exists. It can be seen in Fig. 3.3(b), the states to which the oscillating dynamics collapse to, in turn oscillate with time. It can be concluded that for time-dependent detuning, there exists no steady state.

To analyze this behavior in more detail, this setup is studied for different decay rates (Fig. 3.4). The decay rate decides how fast the states attain the ground dressed state population. Hence, smaller the decay rate, longer it takes. This is clarified by Fig. 3.4; first, the oscillation of the pseudo steady state is similar to that of the detuning and second, by decreasing the decay rate, the pseudo steady state are different. We expect that by increasing our analysis to large time, the states for both decay rates should appear same. Finally, a Fourier Analysis is done to obtain further information.

In the presence of detuning, the effective Rabi frequency is defined as —

$$\Omega_{eff} = \sqrt{\Omega^2 + \Delta^2} = \sqrt{\Omega^2 + \Delta^2(t)} \tag{3.2}$$

For a constant detuning, the Ω_{eff} is a constant and the Fourier analysis should provide us with one sharp peak, whereas a time-dependent detuning would lead to a time-dependent Ω_{eff} and hence multiple peaks in the Fourier analysis.

Fig. 3.5 confirms our claims; we see the presence of multiple peaks for time-dependent detuning and a sharp peak for a constant detuning. A similar analysis for two atoms achieves the same trend. In this extension, the increase in the number of atoms do not lead to any new dynamics.

As mentioned before, the motivation to explore this was to see interesting dynamics. We did come across unique excitation dynamics, i.e. a method to alter the range of the state population dynamics as a function of time. It provided us with a tool to vary the suppression of the excited state as a function of time. Although a simple cosine dependence is considered, there can be other functions (for instance: Gaussian) to get interesting population dynamics. This can even lead to interesting entanglement and effective interaction when we start considering the Rydberg atoms. We also concluded that for such dynamics there are no steady states, and the states tend to oscillate with a similar dynamics as the detuning. The time-dependence was a simple cosine dependence and yet the physics attained is quite interesting. Different functions of time can provide even more interesting features to the simple two-level system. In tune with this, we explore a time-dependent Rabi frequency to examine the possibility of uncovering such unique behaviors.

3.1.1.2 Extension to Time dependent Rabi Frequency

We then extend the system to a time-dependent Rabi frequency, which is defined as —

$$\Omega(t) = \Omega_0(1 + 2\alpha\cos(\omega t)) \tag{3.3}$$

Rabi frequency is the frequency of oscillation. If the Rabi frequency changes, the frequency of oscillation will change. This can be seen in Fig. 3.6 — as the Rabi frequency is time-dependent, the frequency of oscillation also changes with time. Similar to the dynamics of time-dependent detuning, we explore the impact of the different parameters present in the equation on the excitation dynamics. To begin with, we can conclude that the parameter ω will simply increase or decrease the period of the fluctuation in the frequency of oscillation and Ω_0 will increase the effect of α and additionally increase the oscillation frequency. Hence, for this aspect, we prioritize studying the effect of α and detuning on the excitation dynamics. The α value modifies the extent of the oscillation of Ω(t) with time i.e. for $\alpha = 1/4$, Ω(t) varies from 1.5 to 0.5 ($\Omega_0 = 1$), whereas for $\alpha = 1/2$, it varies from 2 to 0 ($\Omega_0 = 1$). Hence, the time-dependence of the frequency of oscillation is more significant for higher α.

This is seen in Fig. 3.7(a) and (b), it demonstrates a behavior called collapse and revival, which is seen previously in coherent field and also hinted at in our analysis of interacting atoms. In this case, neither is this behavior a surprise, as we introduced the cosine dependence that led to this, nor is the dynamics as visually appealing as in the systems stated above. Regardless, it sill provides us with a simple tool to induce the collapse and revival behavior in the Rabi oscillations.

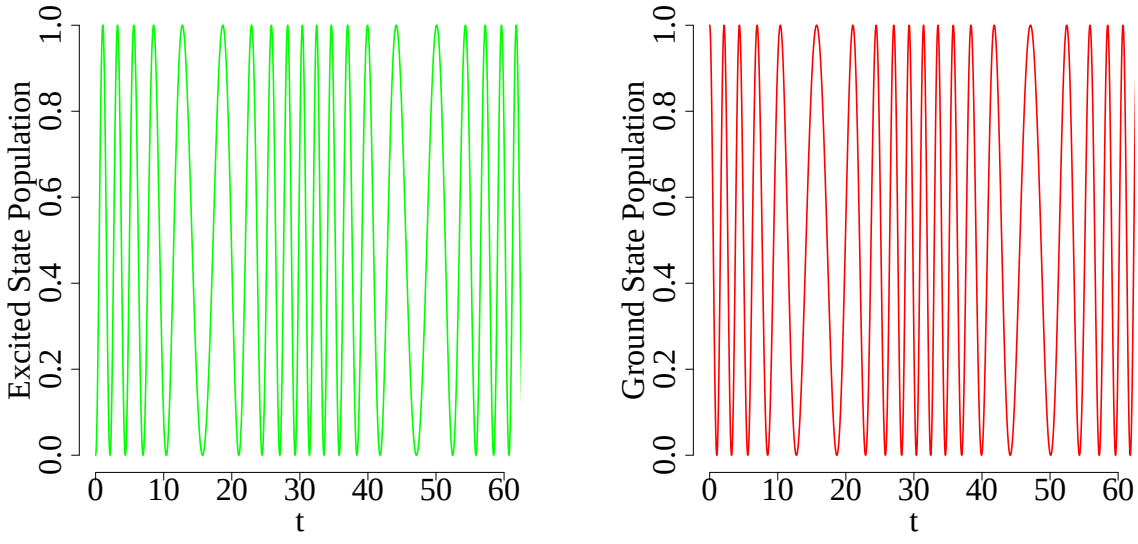

(a) Excited state population **(b)** Ground-state population

Fig. 3.6: Resonant excited state and ground-state dynamics are analyzed for $\Omega(t) = (1 + 2(1/4)\cos((2)(0.1)t))$. We see a fluctuation of the frequency of oscillation in time.

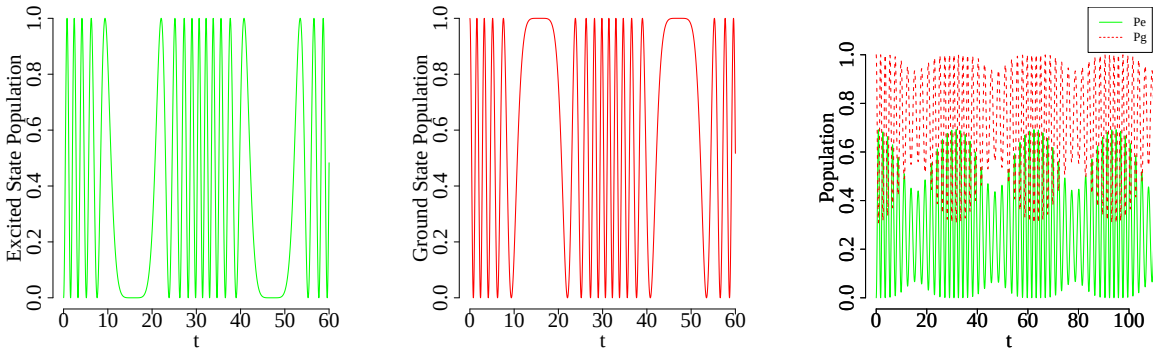

(a) α varied **(b)** α varied **(c)** Detuning is introduced

Fig. 3.7: Ground-state and excited state dynamics are analyzed by varying α in (a) and (b), and by introducing a detuning in (c). The parameters considered for (a) and (b) are $\Omega(t) = (1+2(1/2)\cos((2)(0.1)t))$ and Δ =0. Collapse and revival behavior is seen with the increase in α. The parameters considered for (c) are $\Omega(t) = (1+2(1/4)\cos((2)(0.1)t))$ and Δ =1. With the inclusion of detuning, the envelope behavior appears.

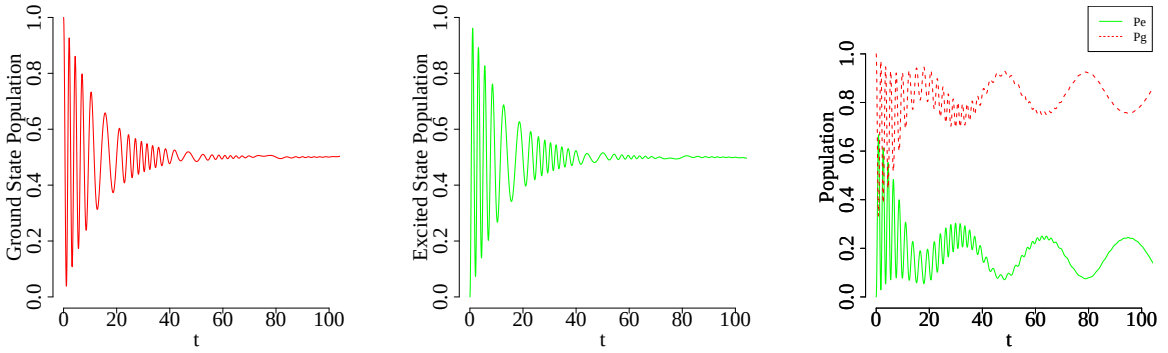

(a) $\Delta = 0$ **(b)** $\Delta = 0$ **(c)** $\Delta = 1\Omega$

Fig. 3.8: Dissipative Rabi Oscillations are studied in the absence and presence of detuning, keeping decay rate $\gamma = 0.1$. For resonant transition, the steady state is constant. The presence of detuning leads to oscillatory steady state.

The analysis of the addition of detuning to this system is not as trivial as previous analyses, i.e. detuning altering the frequency of oscillation. The Rabi frequency couples the two states; higher the frequency, stronger the coupling between the states. Stronger coupling implies more transition to the excited state. We observed earlier that detuning will suppress the excited state population and alter the amplitude. Therefore, when the coupling gets weaker, the suppression due to the detuning becomes stronger. This leads to the envelope behavior seen in Fig. 3.7(c).

The same system is studied in the presence of dissipation. In the Fig. 3.8(a) and (b), the ground-state and excited state are studied in the presence of no detuning. We observe that the fluctuations in the frequency of Rabi oscillations oscillate with time, but once the steady state is attained, they appear to stop. This can be understood by studying the ground dressed state of time-dependent Rabi frequency for resonant transition. The ground dressed state is constant in time with equal population in both the ground and excited state. With the inclusion of a detuning Fig. 3.8(c) which is constant in time, the steady state starts to oscillate in time. This behavior is similar to that of the time-dependent detuning.

Finally, Fourier analysis of the above system is done. As the Rabi frequency or frequency of oscillation is time-dependent, there are many frequencies of oscillation in the time domain being studied. Evident in Fig. 3.9 is one sharp peak for constant Ω but multiple peaks for Ω(t).

A similar analysis is done for two atoms and same trend is attained. Hence, even in this extension the number of atoms do not affect the dynamics. We have obtained an interesting way to alter the oscillation and introduce new behavior. A cosine dependence is quite basic and we still get interesting behaviors such as collapse and revival and envelope behavior. As stated previously, to explore such behaviors, a time-dependent Rabi frequency is the not the only way. There are different ways where this can be achieved, such as a coherent field state or introducing Rydberg states and Rydberg interactions, as seen earlier. Therefore, while studying a classical field more interesting physics is seen with the inclusion of interaction. The interaction induces many interesting features to the systems, i.e. a weak interaction leads to modification of Rabi oscillation to envelopes in the two atom system and hints on proper collapse and revival behavior for many atoms. On the other hand, strong interaction leads to blockade forming collective excited state, which in turn leads to enhancement of Rabi frequency and entanglement. Our goal is to explore many atoms dynamics in the presence of interaction. To attain that, we first explore whether the interesting physics observed still remain in the presence of dissipation.

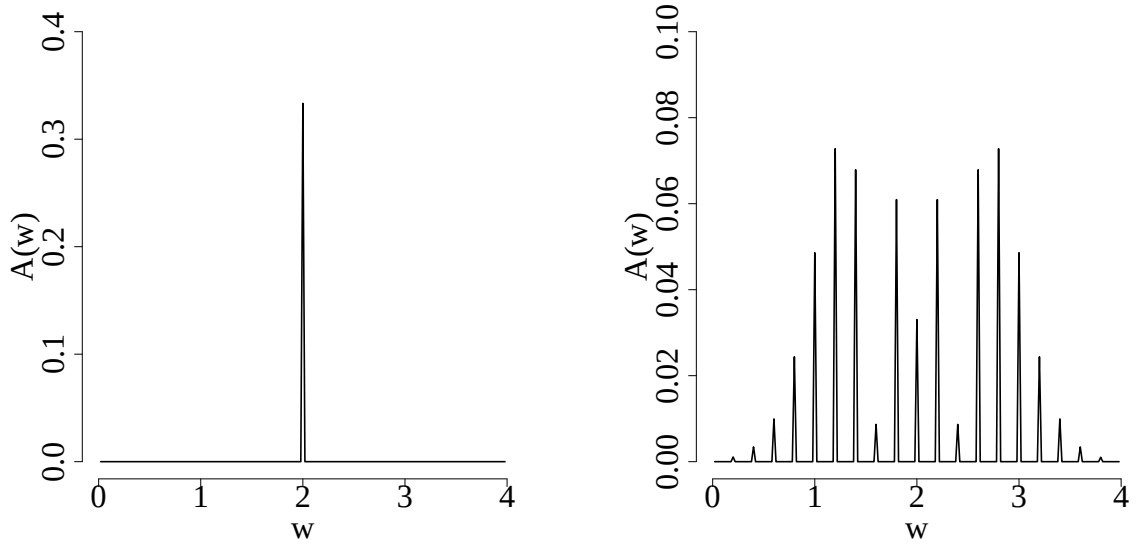

(a) $\Omega = 1$ **(b)** $\Omega(t) = (1 + 2(1/4)\cos((2)(0.1)t))$

Fig. 3.9: Fourier Analysis of Constant Rabi frequency and time-dependent frequency for resonant transition. The presence of multiple peaks are seen in the Fourier analysis of time-dependent Rabi frequency

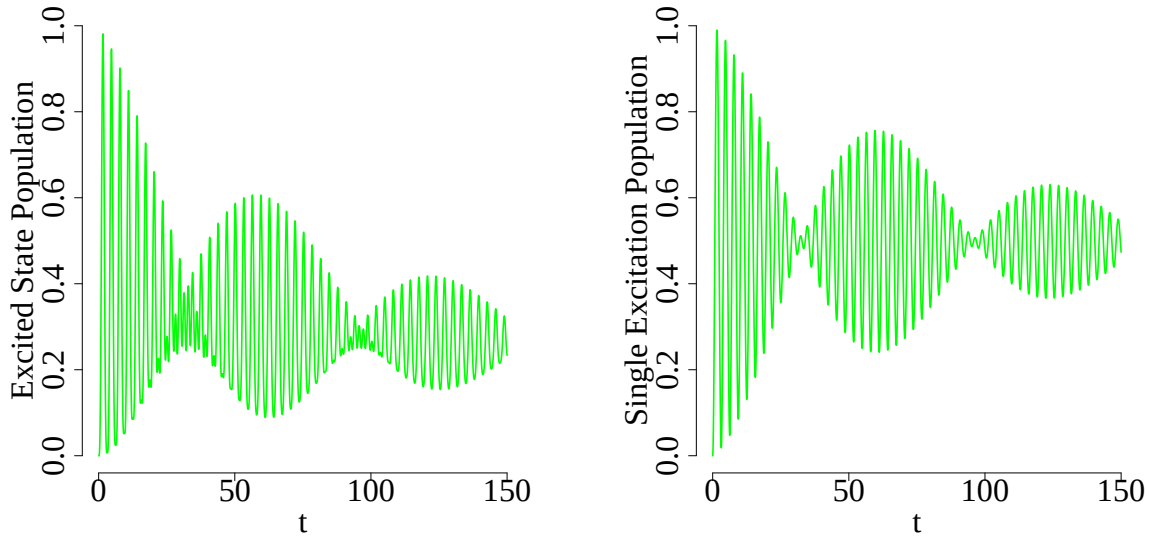

(a) Excited State Population (P_{ee}) **(b)** Single Excitation Population (<P_e>)

Fig. 3.10: The excited state (P_{ee}) and single excitation (<P_e>) dynamics are studied in the presence of weak interaction $V = 0.2\Omega$, weak dissipation $\gamma = 0.01\Omega$ and $\Omega = 1$. All the dynamics are studied for resonant transitions. The envelopes are still visible in the dynamics of decaying system.

3.1.1.3 Interacting excitation dynamics extension to dissipative systems

We have explored the dissipative dynamics in the sections prior to this, but we are yet to explore the excitation dynamics in the presence of interaction for dissipative systems. Thus, we devote ourselves to studying how the excitation dynamics of interacting atoms or the envelope behavior gets affected in the presence of dissipation. Even though the spontaneous emission rate of the Rydberg atom is small due to its long life time, the decay rate is taken to be 0.01Ω. To justify this, we can assume that the Rabi frequency is strong enough to have 0.01Ω as a decay rate of the Rydberg atom. We study the excitation dynamics of two interacting two-level Rydberg atoms.

Fig. 3.10 shows both the single excitation population and multiple excitation population dynamics in the presence of weak interaction strength. It is known that the non-dissipative dynamics of this system show the existence of envelopes in the presence of weak interaction. This envelope nature is preserved in the presence of dissipation. The states decay to their steady state keeping the envelopes intact. The envelopes disappear in the presence of a strong interaction; the dissipation merely leads the oscillating states to their steady state.

This can be seen in Fig. 3.11. Often, systems need to be studied for long durations, sometimes greater than the lifetime of Rydberg atoms; the aim is to ensure the interaction induced physics is preserved. Our analysis informs us that the dissipation does not destroy the interesting dynamics.

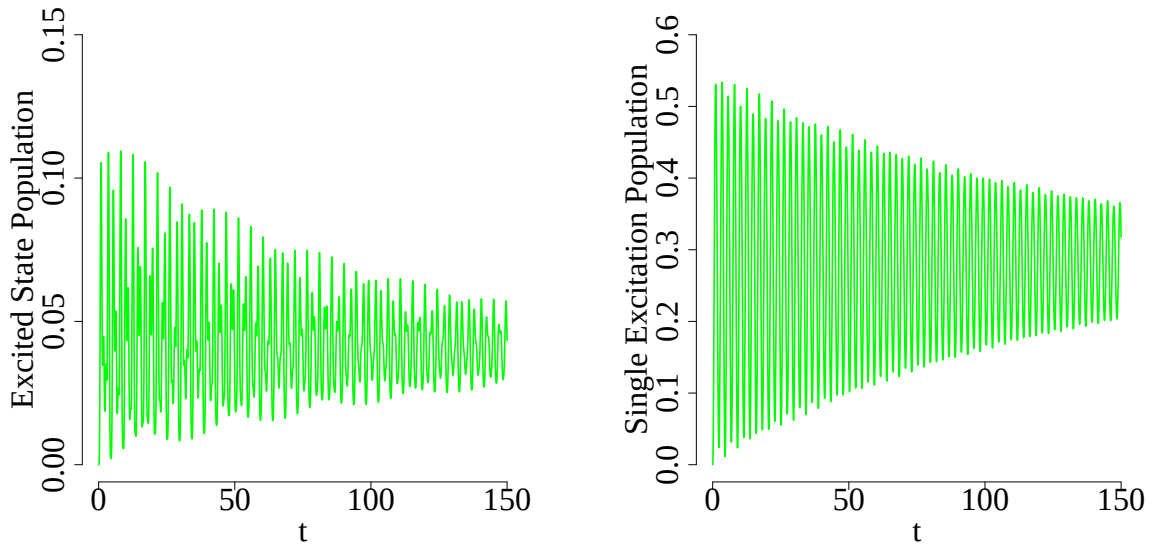

(a) Excited State Population (P_{ee}) **(b)** Single Excitation Population (<P_e>)

Fig. 3.11: The excited state (P_{ee}) and single excitation (<P_e>) dynamics are studied in the presence of strong interaction V = 5Ω and weak dissipation $\gamma = 0.01\Omega$. All the dynamics are studied for resonant transitions. The envelope behavior is not as pronounced.

3.1.1.4 Three Atoms

Rydberg atoms are quite interesting and generate novel dynamics in many-body systems. Thus, as mentioned previously, our goal is to extend our analysis of two interacting atoms to many interacting atoms.

To begin with, we first extend to three atoms and then many atoms. The excitation dynamics of three atoms shows interesting behavior, which has been analyzed and explained in detail [49], so we analyze the effective interaction.

Fig. 3.12 shows effective interaction for three atoms. A similar trend is seen as in the case of two atoms, with three key differences. The first difference is the effective interaction for smaller separation is much stronger compared to two atoms system. This is intuitive as higher number of atoms implies more interaction. The second difference is the decrease of the plateau region (defined as critical radius R_c) of the three atoms when compared to the soft-core potential attained for two atoms. This behavior hints that the blockade radius decreases as the number of atoms increase from two to three. Finally, the third difference is the presence of bumps in three atoms effective interaction, this is due to the inclusion of different types of interactions – nearest neighbor and non-nearest neighbor interactions.

Even though the dressed interaction is of importance to us, the interaction for a non-dressed state also shows comparable change in trend. We observe, other than the change in the interaction strength, not much differs between dressed and non-dressed effective interaction.

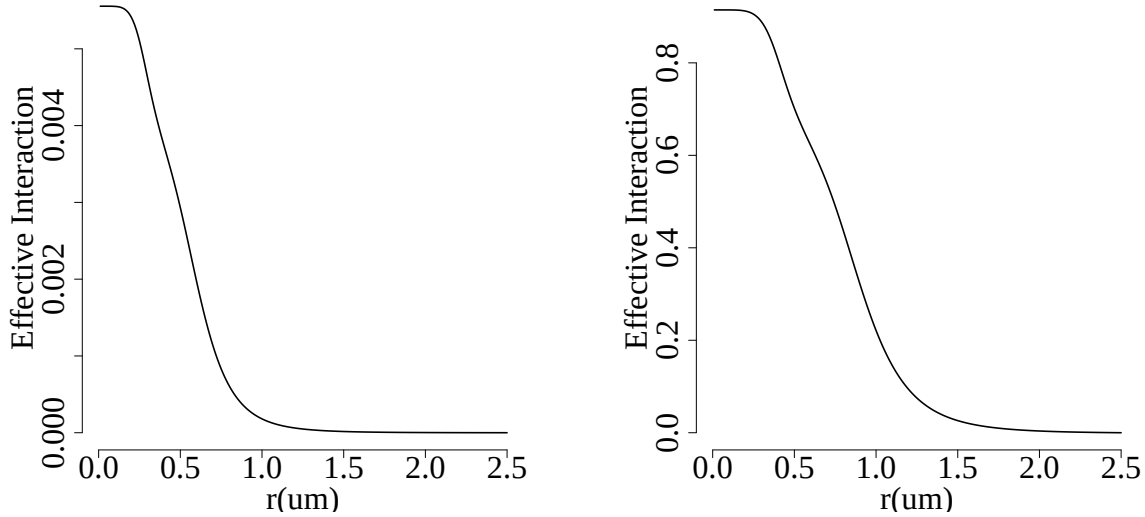

(a) $\Omega/\Delta = 0.2$ **(b)** $\Omega/\Delta = 5$

Fig. 3.12: The effective interaction is computed for different dressing parameter, keeping Ω =1 and $C_6 = \Omega$ and is scaled using the Rabi frequency Ω.

3.1.1.5 Extension to Many Atoms

In this section using the knowledge developed earlier, the excitation dynamics and effective interaction are compared for different number of atoms.

3.1.1.5.1 Excitation Dynamics

The single excitation dynamics is studied for different number of atoms (N = 2, 3, 5, and 10). The single excitation population provides much more physics in comparison to excited state population for higher number of atoms, as even in the presence of weak interactions, the population will be less on account of the presence of large number of states. From Fig. 3.13, it can be seen that with the increase in the number of atoms, the proper envelope behavior of the oscillation due to interaction gets modified. The appearance of the collapse and revival behavior is seen. As mentioned previously, even without considering a time-dependent Rabi frequency, the oscillations can be collapsed and revived. By increasing the number of atoms, the number of excitation channels (number of pathways to the excited state) increase and leads to a destructive and constructive interference between these multiple channels. This interference leads to the collapse and revival of the oscillations in this system. For N = 10, the collapse and revival behavior is similar to the coherent field dynamics. We know that this trait of coherent field has a lot of applications in quantum information science, particularly with induction of entanglement. Therefore, our analysis provides us with another possible application of Rydberg atoms. We now proceed to the analysis of the many-body system — the study of effective interaction.

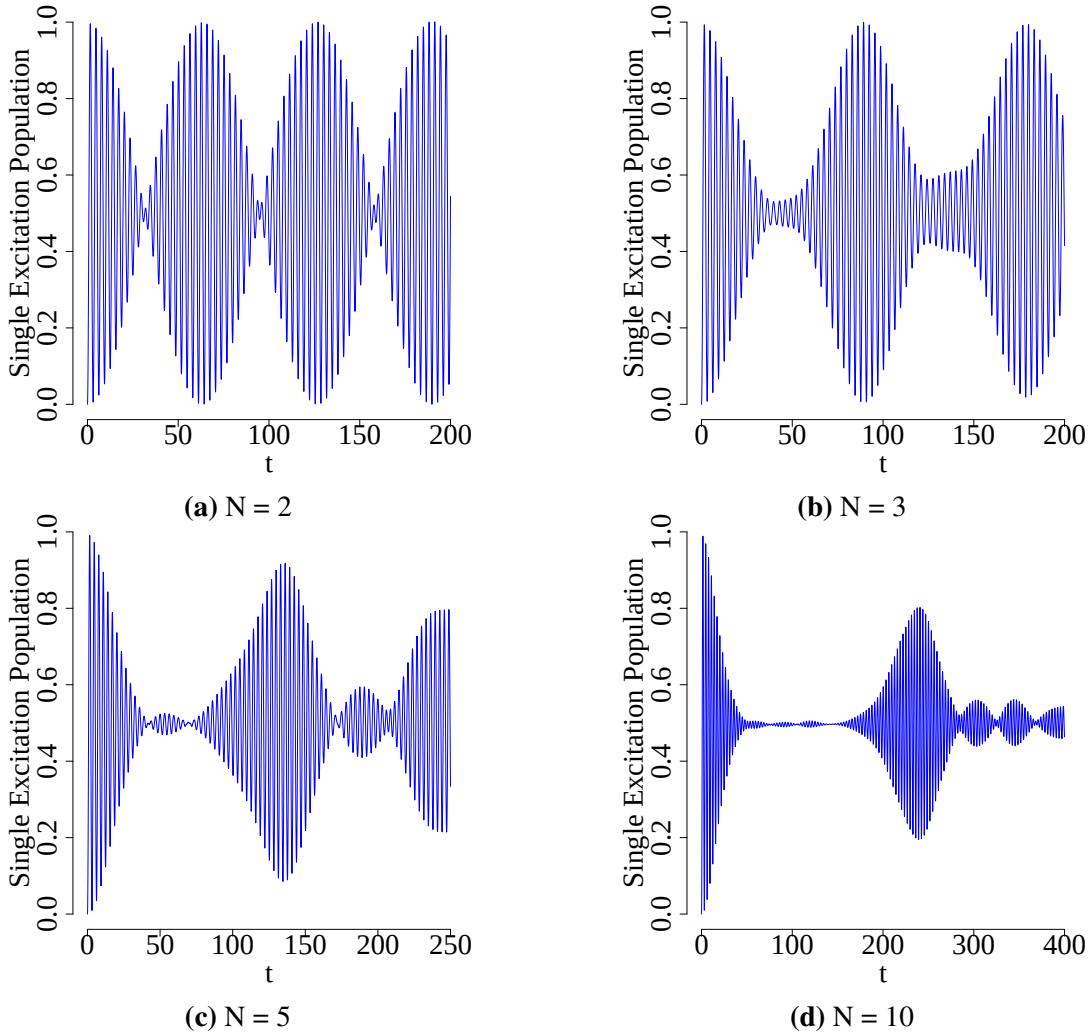

(a) N = 2 **(b)** N = 3

(c) N = 5 **(d)** N = 10

Fig. 3.13: The single excitation dynamics of different number (N) of atoms for $\Omega = 1$, $\Delta = 0$, and $V = 0.2\Omega$. The appearance of collapse and revival of Rabi oscillations is seen for N = 5 and 10.

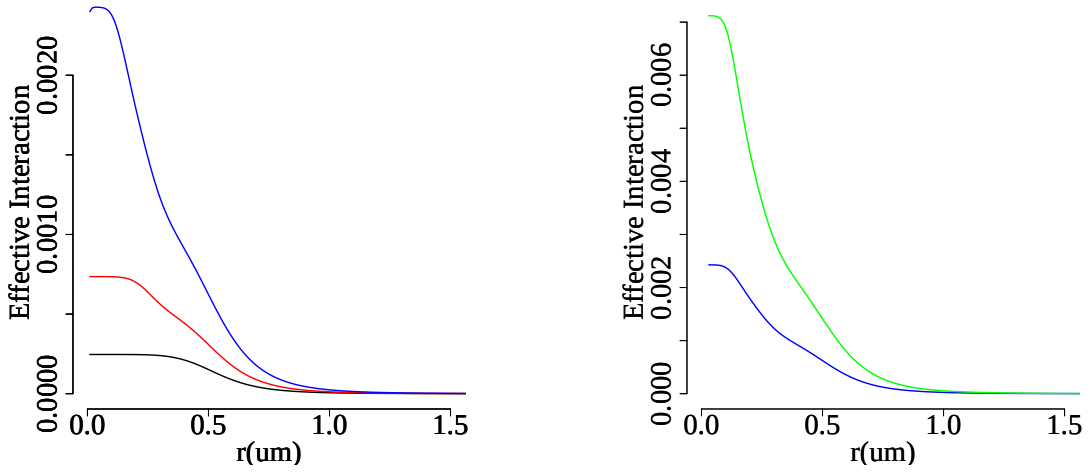

(a) N = 2(Black), 3(Red) and 5(Blue) **(b)** N = 5 (Blue) and 10 (Green)

Fig. 3.14: The effective interaction analyzed above, is computed for dressing parameter Ω/Δ = 0.1. The parameters for the above plots are taken as Ω =1 and $C_6 = \Omega$. The interaction is scaled using Ω.

3.1.1.5.2 Effective Interaction

We saw some interesting results in the analysis of effective interaction, when we went from two atoms to three atoms. We expect to see the differences attained between the two systems to get enhanced with further increase in the number of atoms. The effective interaction is calculated for different number of atoms (N = 2, 3, 5, and 10) in the dressing limit ($\Omega \ll \Delta$). In Fig. 3.14, it can be seen that as the number of atoms increases, the effective interaction also increases. This can easily be explained, as with the increase in the number of Rydberg atoms the interaction increases. Another interesting feature observed is the unique shape of the dressing potential or the soft-core potential, which is seen in two atoms case, gets distorted as the number of atoms increase. The plateau region of the soft-core curve keeps getting smaller as the number of atoms increase, until almost negligible. It is expected as the number of atoms increase further, the soft-core potential may no longer be visible and the potential may appear misleadingly diverging for small r. One point to be noted here is that, the decrease in th critical radius with the increase in the number of atoms, decreases as N increases. With further increase in N, R_c should become constant. Even the bumps, appear with the increase in the number of atoms. This can be clearly seen in the Fig. 3.14. This analysis provides us with some interesting conclusions. However, regarding the relation between the blockade radius and the number of atoms, the analysis still remains inconclusive. To obtain a better understanding of this relation, we explore the multiple excitation probability.

3.1.1.5.3 Multiple Excitation Probability

We made several observations regarding the vanishing nature of the soft-core potential, but nothing definite regarding the blockade radius and how it is affected with the increase in number of atoms. To analyze the change in Rydberg blockade radius, the multiple excitation probability ($<P_{ee}>$) is plot as a function of separation for different number of atoms. Fig. 3.15 shows the probability of finding at least two atoms in the excited state.

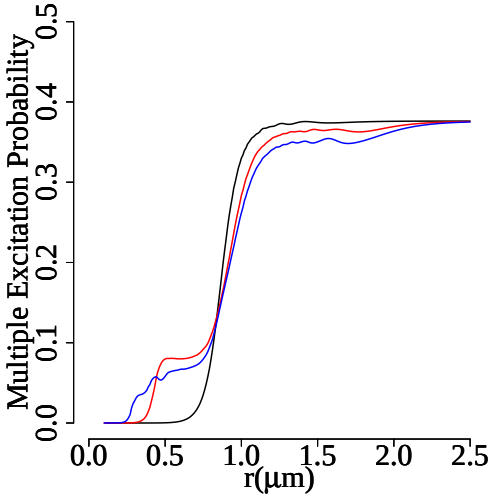

Fig. 3.15: Multiple Excitation Probability ($<P_{ee}>$) for N = 2 (Black), 3 (Red), and 4 (Blue). This is computed for $\Omega = 1$, $C_6 = \Omega$, and $\Delta = 0$

The probability should remain zero within the blockade radius; this can be used to define a blockade radius for N atoms system. It is clear that the blockade radius decreases as the number of atoms increases [47]. Intuition tells us the blockade radius should increase with the number of atoms, but it is on the contrary. With the increase in the number of atoms, the number of interaction increases, but this increase does not lead to the additive increase in the interaction strength. The interactions interfere destructively and thus, the blockade radius decreases.

With this, we conclude our analysis of atoms in a classical field. The classical field provides us with interesting novel dynamics, when we extend our system to time-dependent detuning or Rabi frequency, or when the system of two interacting atoms is extended to many atoms.

We now move on to atoms in a quantized field and carry out similar analyses. The area of interacting atoms quantized field or more coherent field state is still highly unexplored and we aim to gain some insight into these dynamics.

3.1.2 Atoms in Quantized Field

Quantized field promises us exciting dynamics. Also, much of it is unexplored. Most studies in this area are related to entanglement — two non–interacting atoms in a cavity, or studying the effects of coherent field state in quantum information science. Some studies are even based on reproducing JCM using Rydberg atoms. To summarize, a lot of the studies are limited to one atom in a quantized Fock or coherent field or non–interacting atoms in a quantized field.

Hence, in this aspect of the thesis, we begin with exploring simple excitation dynamics with the increase in number of atoms, in the presence and absence of detuning and in the presence and absence of interaction. In addition, as dressed interactions are quite recently studied for classical field, dressed interactions in quantized field provide an exciting scope of research. We aim to explore these interactions. Finally, we repeat some analysis done for classical field with the consideration of quantized field and examine how the physics changes.

3.1.2.1 Two Atoms

The Jaynes–Cummings model we employed in studying the atom–light interactions for quantized field represented by Fock state is extended to two atoms.

The Hamiltonian for this system, using the basis set $|g,g,n+2\rangle$, $|g,e,n+1\rangle$, $|e,g,n+1\rangle$ and $|e,e,n\rangle$ is —

$$\mathscr{H} = \begin{pmatrix} 0 & g\sqrt{n+2} & g\sqrt{n+2} & 0 \\ g\sqrt{n+2} & \Delta & 0 & g\sqrt{n+1} \\ g\sqrt{n+2} & 0 & \Delta & g\sqrt{n+1} \\ 0 & g\sqrt{n+1} & g\sqrt{n+1} & 2\Delta \end{pmatrix}$$

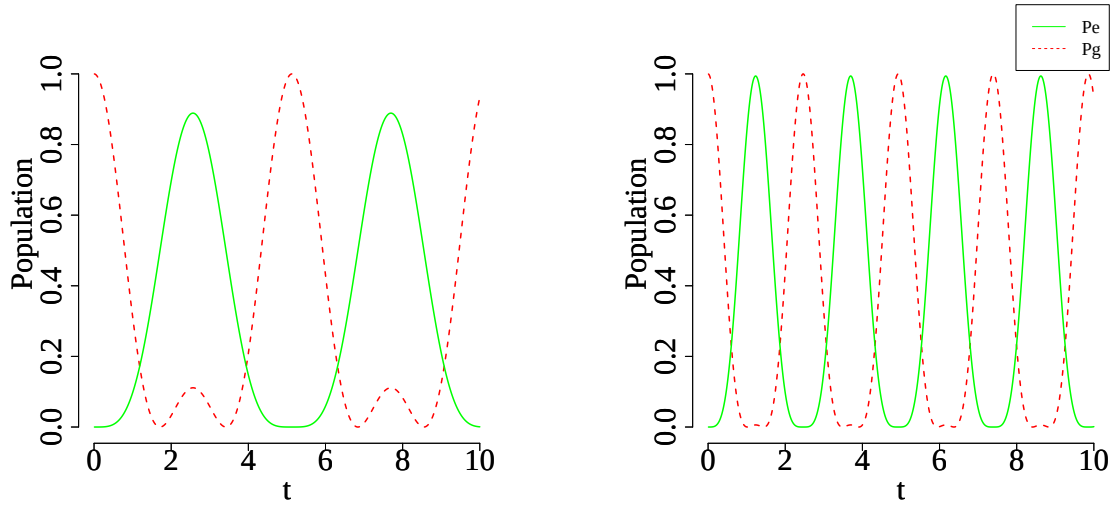

(a) n = 2 **(b)** n = 7

Fig. 3.16: Ground-state and Excited state dynamics for different photon numbers (n = 2 and 7), keeping g =1 and $\Delta = 0$.

Using the Hamiltonian defined above for two atoms, the Rabi oscillation are analyzed for different number of photons (n = 2 and 7). In Fig. 3.16, it can be clearly seen that for less number of photons, a unique behavior arises in the ground-state population which is not seen in the classical field picture. As the number of photons increase, this behavior vanishes. From the equations derived above, it can be clearly seen that for two atoms, there are two Rabi frequencies defined — $2g\sqrt{n+2}$ and $2g\sqrt{n+1}$. The difference between these frequencies is more apparent for a small number of photons. This dynamics is more pronounced for higher number of atoms, as with the increase in the number of atoms, the number of Rabi frequencies increases (as we see later). It is expected for N atoms N frequencies exist. These Rabi oscillations are studied further in the presence of detuning ($\Delta = 0.2\Omega_n$) for n = 2 and 7 Fig. 3.17. The Rabi oscillations get modified to form envelopes, as seen in the case of two interacting atoms. This kind of behavior is unique to such a system. The Fourier analysis of resonant n = 2 dynamics, shows two peaks that correspond to the two Rabi frequencies. If the value of n is increased, the peaks combine. On addition of a weak detuning ($\Delta = 0.2\Omega_n$), the peak corresponding to the smaller frequency splits into two peaks. The detuning also shifts the two primary peaks. As the detuning is increased to intermediate values, the two peaks, that were formed due to splitting of the smaller frequency, spread with one shifting towards zero and the other shifting towards the second primary peak. Finally, when the detuning is increased to large values, the Fourier analysis shows only one peak. One can assume that the peak shifting towards zero will reach zero and the other peak will combine with the second primary peak. Another way of explaining is that strong detuning will lead to an effective Rabi frequency that is same for both the Rabi frequencies, a behavior that happens if the number of photons is increased. With the increase in the number of photons (Fig. 3.17), it can be seen that the period of the envelope increases. Hence, if oscillations were observed for a short time duration, the classical Rabi oscillations would appear with damped amplitudes, but once the time period is increased, envelopes appear.

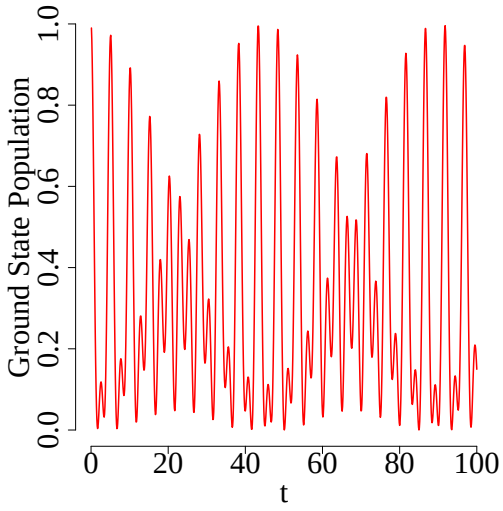

(a) Ground State $n = 2$

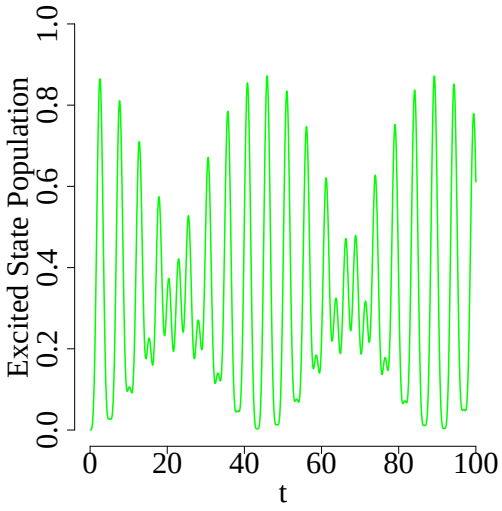

(b) Excited State $n = 2$

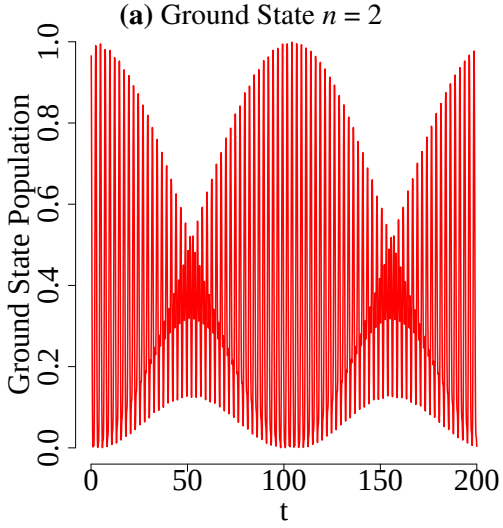

(c) Ground State $n = 7$

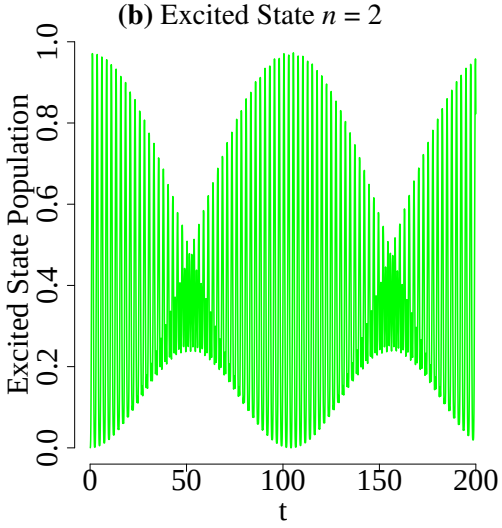

(d) Excited State $n = 7$

Fig. 3.17: Ground-state and Excited state for $n = 2$ and 7, keeping g =1 and $\Delta = 0.2\Omega_n$.

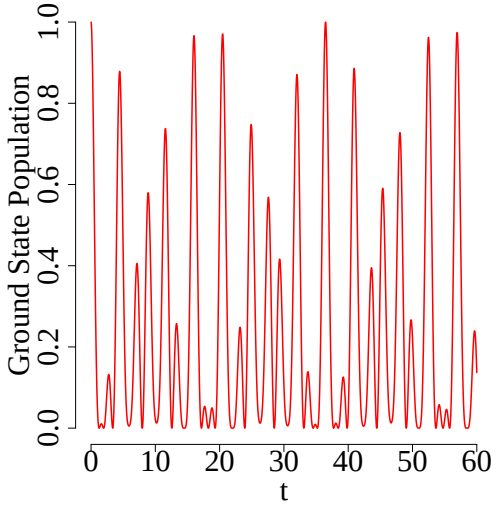

(a) Ground State $n = 3$

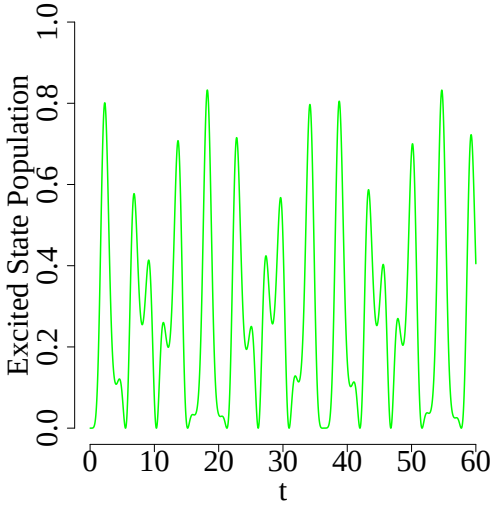

(b) Excited State $n = 3$

Fig. 3.18: Ground-state and Excited state for $n = 3$, keeping g = 1 and $\Delta = 0$.

3.1.2.2 Three Atoms

Similarly, the JCM is extended to three atoms; the Hamiltonian for this system using the basis set $|g,g,g,n+3\rangle$, $|g,g,e,n+2\rangle$, $|g,e,g,n+2\rangle$, $|g,e,e,n+1\rangle$, $|e,g,g,n+2\rangle$, $|e,g,e,n+1\rangle$, $|e,e,g,n+1\rangle$, $|e,e,e,n\rangle$ is given as —

$$\mathscr{H} = \begin{pmatrix} 0 & g\sqrt{n+3} & g\sqrt{n+3} & 0 & g\sqrt{n+3} & 0 & 0 & 0 \\ g\sqrt{n+3} & \Delta & 0 & g\sqrt{n+2} & 0 & g\sqrt{n+2} & 0 & 0 \\ g\sqrt{n+3} & 0 & \Delta & g\sqrt{n+2} & 0 & 0 & g\sqrt{n+2} & 0 \\ 0 & g\sqrt{n+2} & g\sqrt{n+2} & 2\Delta & 0 & 0 & 0 & g\sqrt{n+1} \\ g\sqrt{n+3} & 0 & 0 & 0 & \Delta & g\sqrt{n+2} & g\sqrt{n+2} & 0 \\ 0 & g\sqrt{n+2} & 0 & 0 & g\sqrt{n+2} & 2\Delta & 0 & g\sqrt{n+1} \\ 0 & 0 & g\sqrt{n+2} & 0 & g\sqrt{n+2} & 0 & 2\Delta & g\sqrt{n+1} \\ 0 & 0 & 0 & g\sqrt{n+1} & 0 & g\sqrt{n+1} & g\sqrt{n+1} & 3\Delta \end{pmatrix}$$

The excitation dynamics for the Hamiltonian derived for three atoms is studied for photon numbers n = 3 and 8. The excitation dynamics for three atoms as seen in Fig. 3.18, is quite different to the excitation dynamics of three atoms with classical field. The envelopes, which were missing in two atoms picture in the quantized field or in N atoms picture for classical field, appear. The three Rabi frequencies that arise in this system become prominent in the presence of small number of photons, which interfere to give beats that is seen as an envelope as explained above. It is assumed that if the photon number is increased, the dynamics should reproduce a classical field picture.

From Fig. 3.19, it is well understood that to obtain the envelope nature for large n, one has to increase the time period considered. To obtain the classical picture, the photon numbers have to be kept large enough and the time period has to be kept small enough to get the classical Rabi oscillations.

Previously, in the two atoms case, the detuning modified the simple looking Rabi oscillations into envelopes of oscillations and this was explained by claiming that detuning exaggerated the underlying dynamics of two atoms in the quantized field. In the case of three atoms, the oscillations are already forming an envelope nature. It would be interesting to know how the detuning affects these existing envelopes. For weak detuning (0.2Ω), the dynamics are studied for n = 8 (Fig. 3.20). The addition of the detuning does not destroy the existing defined envelope nature.

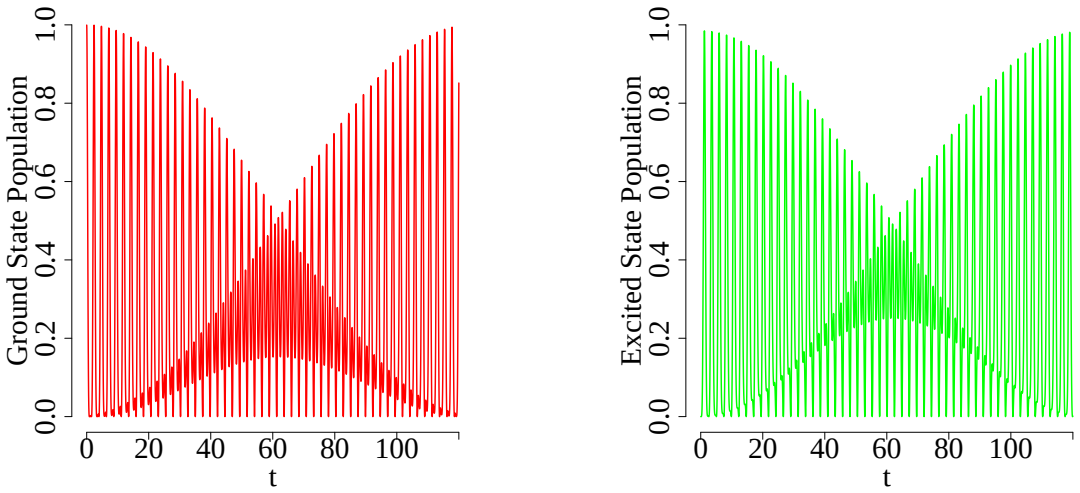

(a) Ground State $n = 8$ **(b)** Excited State $n = 8$

Fig. 3.19: Three atoms resonant Rabi oscillation for quantized field. Ground-state and Excited state for $n = 8$, keeping g = 1 and $\Delta = 0$.

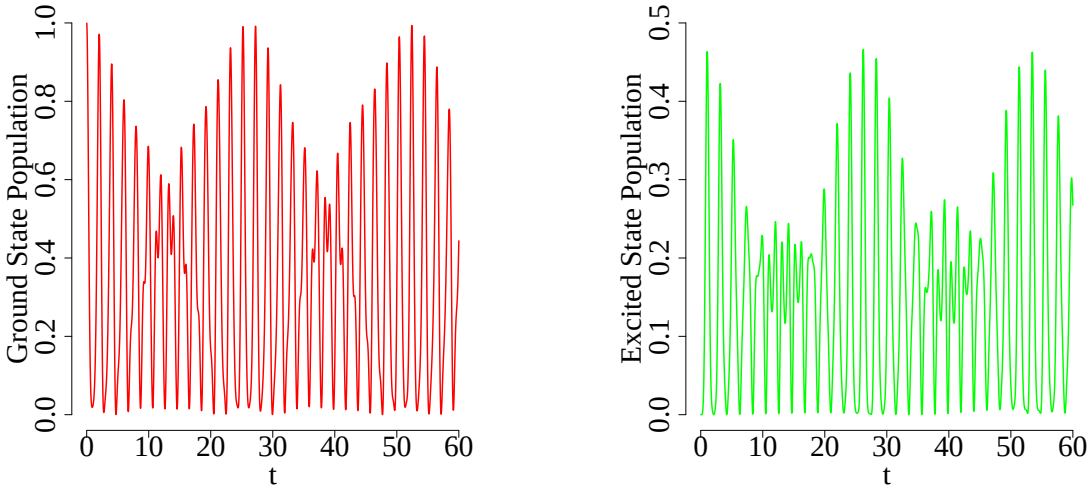

(a) Ground State Population **(b)** Excited State Population

Fig. 3.20: Three atoms non-resonant Rabi oscillation for quantized field. Ground-state and Excited state for $n = 8$, keeping g = 1 and $\Delta = \Omega_n$.

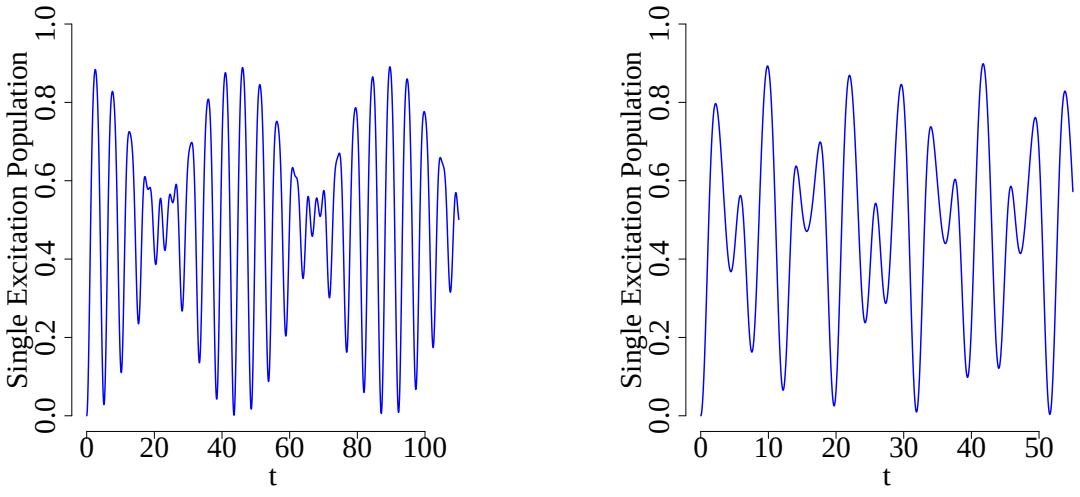

(a) V = $0.2\Omega_n$ **(b)** V = $5\Omega_n$

Fig. 3.21: Single Excitation (<P_e>) dynamics for $n = 2$, keeping g = 1 and $\Delta = 0$.

3.1.2.3 Extension of above systems — Interacting atoms

The above systems are studied in the presence of interaction. For the purpose of maximizing the features arising due to the quantized nature of the field, the number of photons are kept small for the analysis of the excitation dynamics. First, the excitation dynamics for two atoms is analyzed in the presence of interaction: V = 0.2Ω and 5Ω. Fig. 3.21 shows the formation of envelopes for weak interaction as in the case of the classical field. In the presence of strong interaction, the envelopes disappear. With the increase in the number of photons, these envelopes develop a large time period. The behavior is similar to classical field and not unique to the quantized field with the exception that the oscillation range is less than 0–1. This range increases with the number of photons. This analysis of two interacting Rydberg atoms is extended to three atoms.

The excitation dynamics for three atoms is studied in the presence of weak interaction V = 0.2Ω and strong interaction V = 5Ω (Fig. 3.22). We see a similar behavior — formation of envelopes for weak interaction and the behavior becoming erratic for strong interaction. One interesting observation here is that in the case of three weakly interacting atoms in a classical field, the dynamics had multimodal nature, i.e. the nodes of the envelope behavior changed (increased) with time, it also had oscillation ranging from 0–1. The dynamics observed here has no sign of multimodal nature and even the range of oscillation is much less than 0–1, though we can increase the range by increasing the photons.

Even though we do not attain an out-of-the-ordinary or drastic change in behavior, there are features in the dynamics that are unique to the quantized field. We also see a hint of the appearance of collapse and revival behavior in the weak interaction dynamics. This appearance is destroyed with addition of strong interaction. As the extension to many atoms picture interacting with quantized field is not as trivial as in the case of the classical field, the excitation dynamics are so far limited to three atoms. The collapse and revival behavior are further explored in a different field state, the previously defined coherent field state.

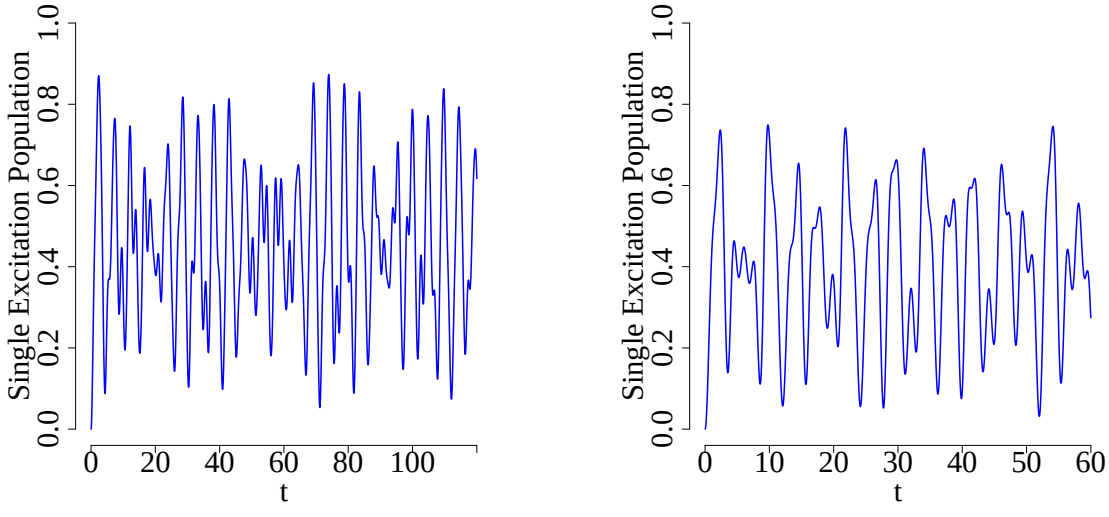

(a) V = $0.2\Omega_n$ **(b)** V = $5\Omega_n$

Fig. 3.22: Single Excitation (<P_e>) dynamics for n = 3, keeping g = 1 and Δ = 0.

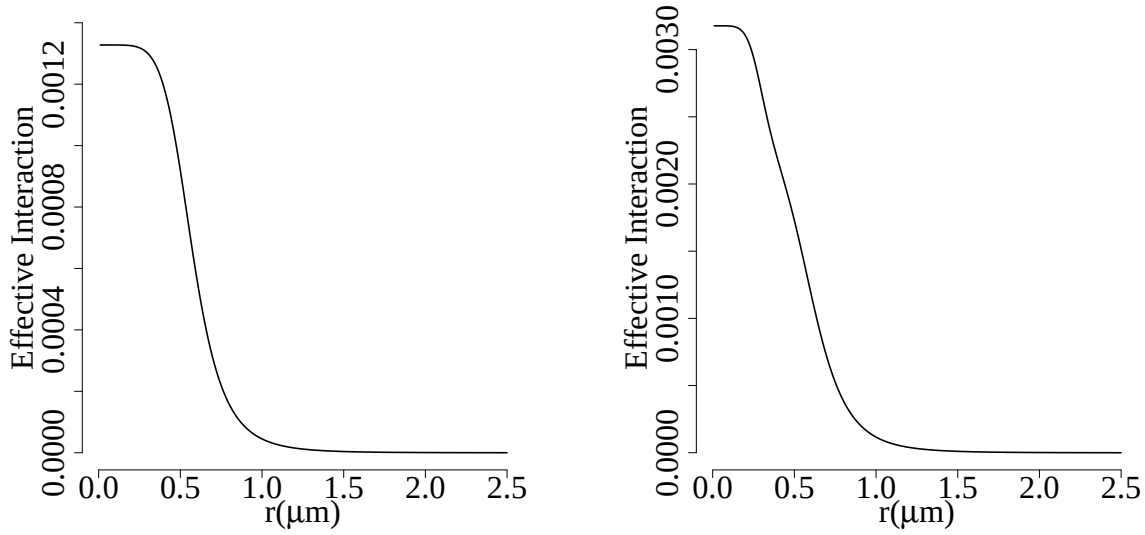

(a) N=2 **(b)** N=3

Fig. 3.23: Effective interaction vs separation for N = 2 and 3, keeping g = 1 and $\Delta = 10\ \Omega_n$.The interaction is scaled by atom field coupling constant g.

3.1.2.4 Extension of above systems — Effective Interaction

Before we conclude the dynamics of atoms in quantized field represented by Fock state, we decided to study the dressed effective interactions of Rydberg atoms. The study of dressed potential is quite recent and hence, this particular extension has not yet been studied. Fig. 3.23 shows the dressed effective interaction for two and three atoms. The trend appears similar to that of the classical field; we explore this in much detail in a later section.

3.1.2.5 Extension of Coherent Field State — Interacting Two and Three atoms

Similar analysis, as in the case of quantized Fock state, is done for two and three atoms in the coherent field state. For this, the knowledge of quantized field Hamiltonian of interacting two and three atoms is combined with the knowledge of coherent field state. To begin with, the single excitation dynamics of resonant non-interacting two atoms is studied (Fig. 3.24(a)). This dynamics is similar to the one atom picture with no changes due to the presence of another atom. To the same resonant system, detuning is added (Fig. 3.24(b)). The addition of detuning does not change the behavior, it only alters the amplitudes of the envelopes, making them smaller. In the Fock field state or classical field, the presence of interaction led to the formation of envelopes. In the coherent field state, the excitation dynamics already has a collapse and revival behavior; with the inclusion of interaction, additional frequencies are introduced (Fig. 3.24(c)). The resulting dynamics is the division of the existing envelopes and formation of new and smaller ones. This is repeated for a higher mean photon number ($\overline{n} = 20$), in Fig. 3.25. With the increase in the mean photon number, the collapse and revival becomes more periodic and pronounced. Hence, the effect of the interaction and the detuning is also quite clearly seen. This analysis is extended to three atoms for $\overline{n} = 20$ and they show a similar behavior, although the trend is much suppressed (Fig. 3.26).

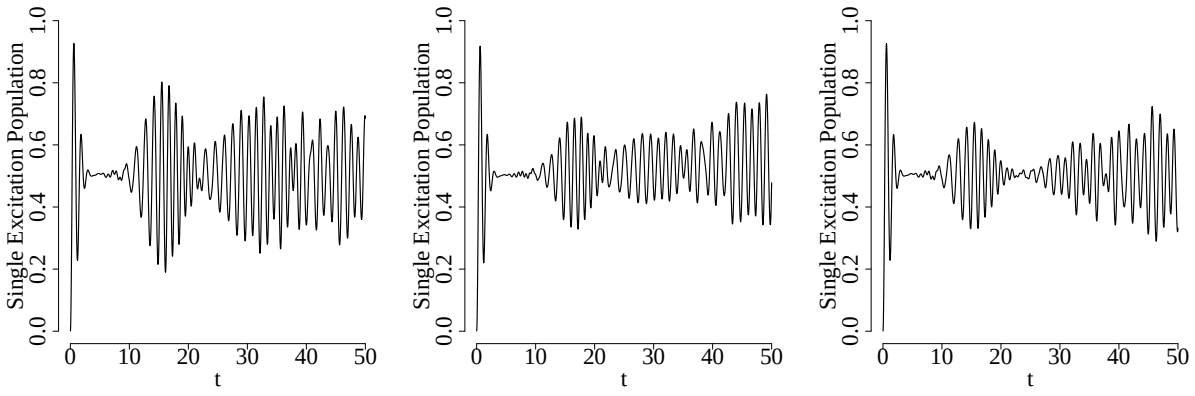

(a) $\Delta = 0$, V = 0 **(b)** $\Delta = 0.2\Omega_{\overline{n}}$, V = 0 **(c)** $\Delta = 0$, V = $0.2\Omega_{\overline{n}}$

Fig. 3.24: Single excitation dynamics for $\overline{n} = 5$, keeping g =1 in the presence and absence of interaction and detuning.

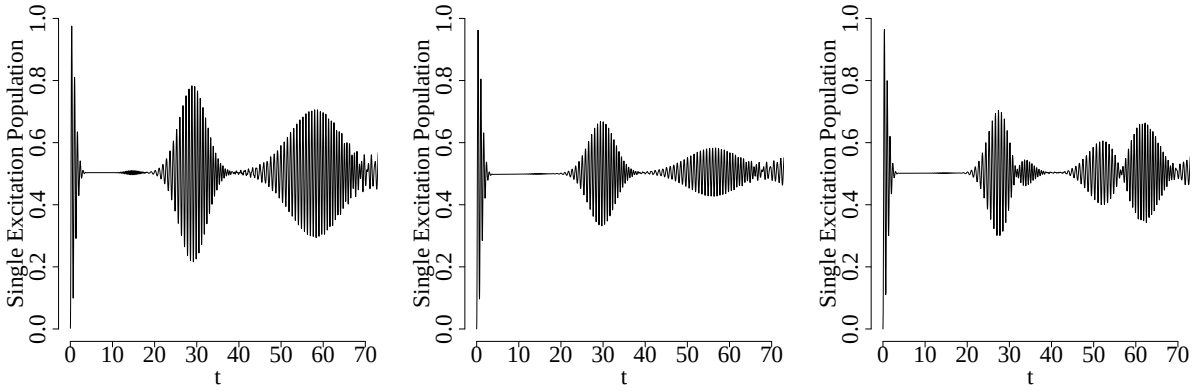

(a) $\Delta = 0$, V = 0 **(b)** $\Delta = 0.2\Omega_{\overline{n}}$, V = 0 **(c)** $\Delta = 0$, V = $0.2\Omega_{\overline{n}}$

Fig. 3.25: Single excitation dynamics for $\overline{n} = 20$, keeping g =1 in the presence and absence of interaction and detuning.

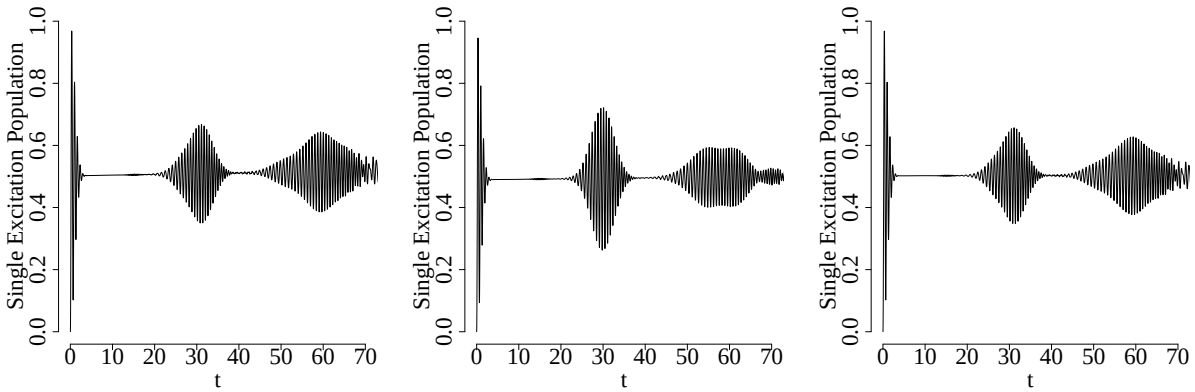

(a) $\Delta = 0$, V = 0 **(b)** $\Delta = 0.2\Omega_{\overline{n}}$, V = 0 **(c)** $\Delta = 0$, V = $0.2\Omega_{\overline{n}}$

Fig. 3.26: Single excitation dynamics for $\overline{n} = 20$, keeping g =1 in the presence and absence of interaction and detuning.

3.1.2.6 Extension of Coherent Field State — Effective Interaction

Before concluding the dynamics of atoms in a quantized coherent field, Fig. 3.27 shows the dressed effective interaction for two and three atoms. The trend appears similar to that of the classical field and the quantized Fock field state. We explore this in greater detail in the section that follows.

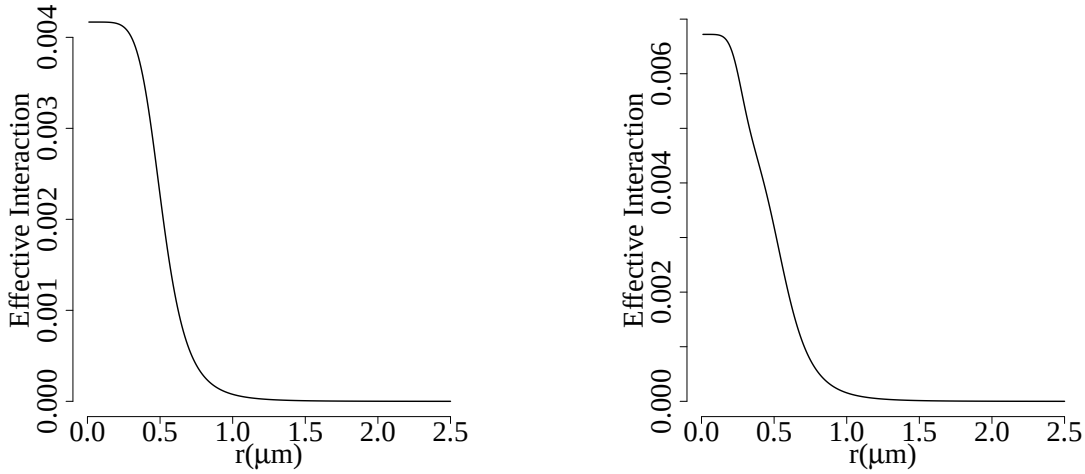

(a) N=2 **(b)** N=3

Fig. 3.27: Effective interaction Vs separation for N = 2 and 3, keeping g = 1 and Δ = 10 Ω_n. The interaction is scaled by g.

3.1.3 Comparison of Effective Interaction for different fields

Fig. 3.28 shows the effective interaction in different fields computed for similar Rabi frequency and dressing parameters. For a quantized field there are two Rabi frequencies for one n and even in case of coherent field there will exist two Rabi frequencies for $\overline{n}$, hence two effective interaction are computed for the classical field for the respective frequencies. It can be clearly seen that both the definitions in the case of classical field result in effective interaction greater than the quantized and the coherent field, the coherent field being the least. With the increase in n or $\overline{n}$, the quantized field and the coherent field come closer and they even come close to the value of the classical field. Similar analysis is done for three atoms (Fig. 3.29), and the same behavior is observed.

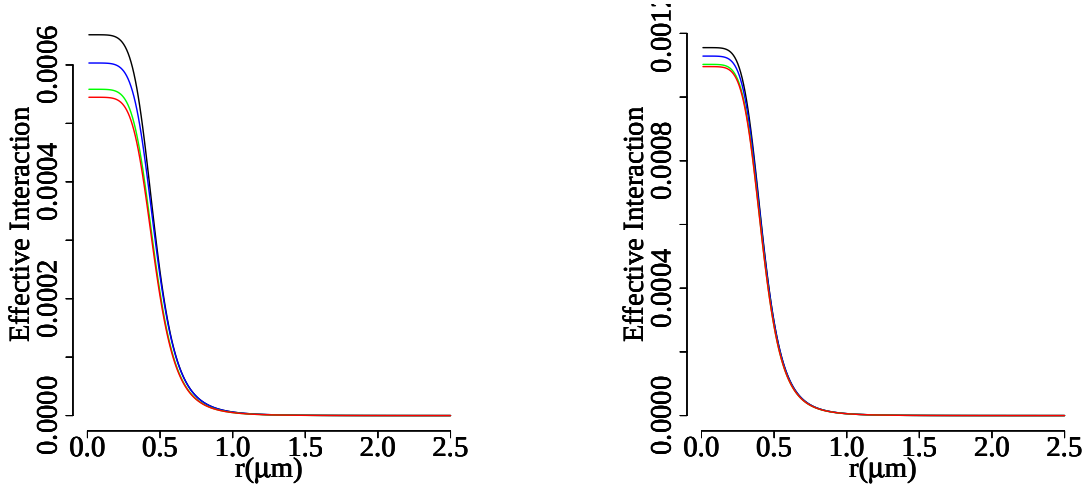

(a) $n = \overline{n} = 5$ **(b)** $n = \overline{n} = 20$

Fig. 3.28: Effective interaction between two atoms is computed for Classical field (Black: Ω = $2g\sqrt{n+2}$, Blue: Ω = $2g\sqrt{n+1}$), Quantized Fock field (Green: Ω_n = $2g\sqrt{n+2}$, $2g\sqrt{n+1}$), and Coherent field (Red: Ω_n = $2g\sqrt{n+2}$, $2g\sqrt{n+1}$) keeping g = 1 and Δ = 10 Ω or 10 Ω_n. The effective interactions are scaled using g.

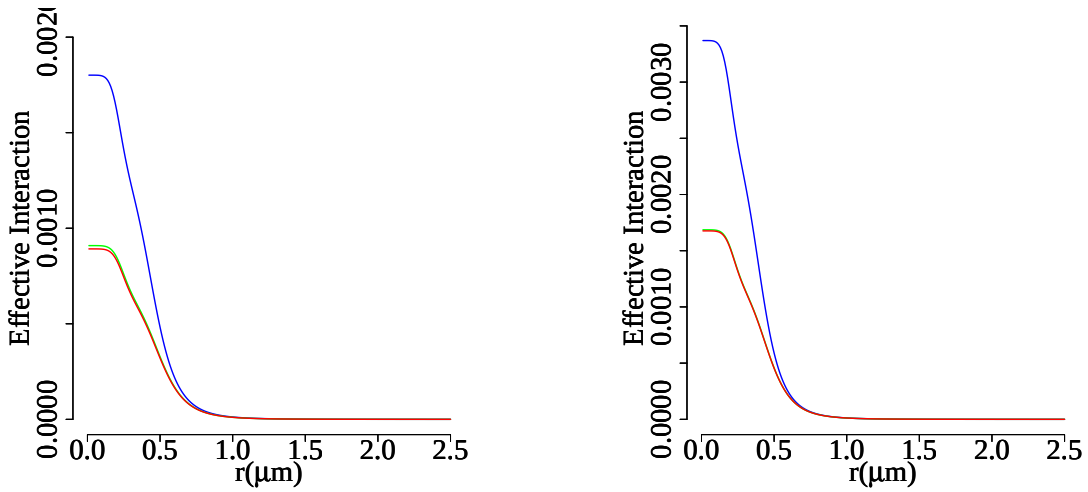

(a) $n = \overline{n} = 5$ **(b)** $n = \overline{n} = 20$

Fig. 3.29: Effective interaction between three atoms is computed for Classical field (Blue: $\Omega = 2g\sqrt{n+1}$), Quantized Fock field (Green: $\Omega_n = 2g\sqrt{n+3}$, $2g\sqrt{n+2}$, $2g\sqrt{n+1}$), and Coherent field (Red: $\Omega_n = 2g\sqrt{n+3}$, $2g\sqrt{n+2}$, $2g\sqrt{n+1}$) keeping g = 1 and $\Delta = 10\ \Omega$ or $10\ \Omega_n$. The effective interactions are scaled using g.

3.1.3.1 Multiple Excitation Probability

Similar analysis like the classical field is done for all the fields to comment on the blockade radius as they can't be formulated for coherent field. The Multiple excitation probability (<P_{ee}>) is plot for the different fields to get an estimate of the blockade radius. Fig. 3.30 shows that in all the three fields the system has the same blockade radius.

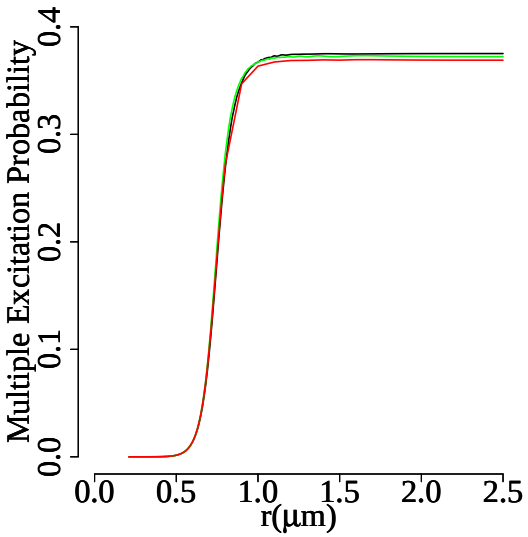

Fig. 3.30: Multiple Excitation Probability (<P_{ee}>) is computed for different fields, keeping $\Omega = 2\sqrt{6}$, $\Delta = 0$ and $C_6 = \Omega$.

Using this, we make some concluding remarks about the many-body dynamics of quantized field. The appearance of correlated many-body physics arising due to strong Rydberg interactions in a classical field is studied. They investigate the scaling behavior of saturated Rydberg fractions, $f_r = N_{ryd}$ which is defined as α^{ν}. α is a dimensionless parameter defined as $\hbar\Omega/C_6\rho^2$,

ρ being the atomic density. In one dimension, they derive the value of ν as 0.150. They used mean field approximation to simplify [21], [55] is used to attain the results numerically. We follow the approach [56] of taking an analytical approximation to attain the same results. The Rydberg fraction N_{ryd} is defined as $\gamma^*(L_{eff}/R_b + 1)$, where γ^* is taken as 0.5 and L_{eff} is taken as (L - ρ^{-1}), L is the length of the sample and R_b is the blockade radius. Hence, it can be concluded that much of the dynamics can be understood by figuring out the blockade radius. If the atomic density and the length of the sample is taken to be same for different systems, then the blockade radius is the sole deciding factor. As can be seen from the multiple excitation probability, the blockade radius for all the three fields are same. Therefore, they should have the same ν. To this end, we have attained interesting features for quantized field in both excitation dynamics and effective interaction. We aim to extend the few body dynamics to many-body dynamics for the quantized field, and are currently working towards it.

3.2 Three-Level Interacting Atoms

As mentioned in the previous chapters, our analysis of the three-level excitation dynamics did not yield any exciting novel dynamics; much of the dynamics is similar to the two-level scheme. Hence, we decided to prioritize the effective interaction. The effective interaction in the case of three-level interacting atoms in a dressed EIT setup leads to exotic curves and existence of maximum at finite separations. Our first aim is to analyze how the position of these maxima can be changed, To do that, we include angular dependence in the C_6 coefficient.

3.2.1 Angular Dependence of C_6

Using the numerical method defined in the previous section for computation of effective interaction for three-level interacting atoms, the total interaction energy is calculated. van der Waals interaction between *np* states is given by [53] —

$$\mathscr{W} = V_{00} = \frac{(ea_0)^4 n^{11} \sin^4(\theta)}{r^6} \text{ and } \mathscr{W} = V_{11} = \frac{(ea_0)^4 n^{11} \cos^4(\theta)}{r^6} \tag{3.4}$$

and for simplicity the C_6 coefficient is taken to have only sine dependence. Fig. 3.31 shows a shift of the effective interaction curve towards the y axis due to the the angular dependence. This behavior is expected, as the angular dependence just decreases the C_6 value. Thus, the van der Waals interaction is lower for a particular *r*. Next, we aim to explore how these dynamics change once we extend the system. The two possible extensions we consider are inclusion of three-body interaction and extension to four-level scheme. We first explore the three-body interactions.

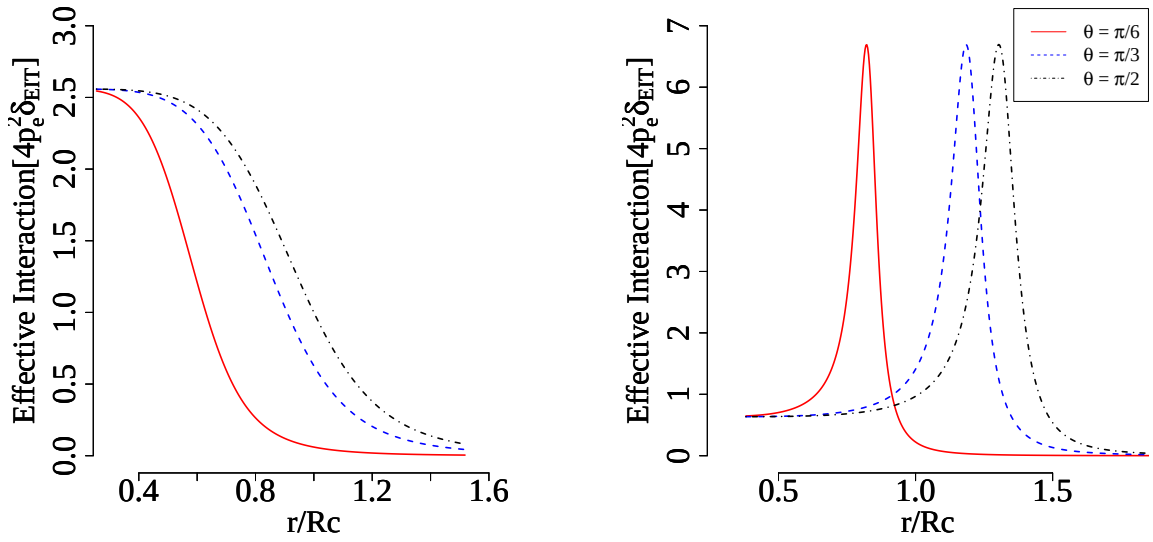

(a) $\Omega/2\Delta_1 = 0.6$ **(b)** $\Omega/2\Delta_1 = 2$

Fig. 3.31: The effective interaction analyzed above, is computed for $\Delta_1/\gamma_p = 2.5$, $\Omega_1/\Omega_2 = 0.1$ and dressing parameters $\Omega/\Delta = 0.6$ and 2. The values of $\theta = \pi/6$ (Red), $\pi/3$ (Blue) and $\pi/2$ (Black). The decay rate γ is taken as 1.

3.2.2 3-body Interaction

The three body interaction is given by [54] as —

$$\mathscr{W}_{ijk} = \frac{C_9(1+3(\cos(\theta)^3))}{r^9}\hat{\sigma}^1_{ee} \otimes \hat{\sigma}^2_{ee} \otimes \hat{\sigma}^3_{ee} \tag{3.5}$$

where $C_9 \approx \sqrt{C_6^3}$.

In this section, the three-body interactions are computed for two different configurations.

3.2.2.1 Equilateral Triangle

Consider 3 three-level atoms forming an equilateral triangle. They interact via van der Waals interaction: V_2 as the two-body interaction and V_3 as the three-body interaction.

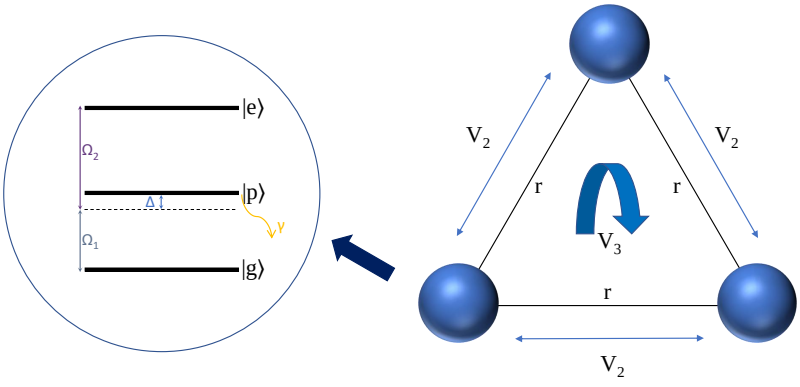

Fig. 3.32: Equilateral triangle configuration.

The effective interaction curve (Fig. 3.33) is similar to the two-body interactions. The ground-state population curve informs that most of the population is in the ground-state. Therefore, the interaction curve should take up a soft-core potential like it does in the case of two-interacting atoms. It appears to take up a soft-core potential for $\Omega_2/2\Delta_1 < 1$, like it does in the two interacting atoms case. Similarly, for $\Omega_2/2\Delta_1 > 1$, there is one defined maximum like in the case of two interacting atoms. Hence, the effect of the three-body interaction is not significant in this configuration. The ground-state population and the effective interaction suggests that unlike the two-body interaction case, the initial maximum occurs for $\Omega_2/2\Delta_1 = 1.1$ instead of 1.

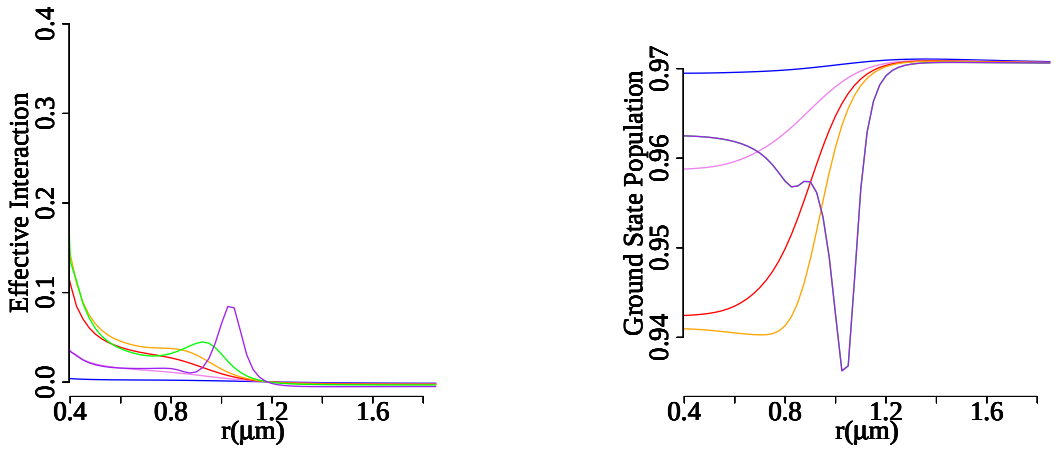

Fig. 3.33: The effective interaction and ground-state population for $\Delta_1/\gamma_p = 2.5$, $\Omega_1/\Omega_2 = 0.1$ and varying dressing parameters $\Omega/2\Delta_1 = 0.6$ (Blue), 0.85 (Pink), 1 (Red), 1.1 (Orange), 1.3 (Green) and 2 (Purple). Decay rate γ is taken as 1. The effective interactions are scaled using the decay rate.

3.2.2.2 One-dimensional Linear Chain

Consider 3 three-level atoms forming a 1D linear chain. They interact via van der Waals interaction: V_2 as the two-body interaction and V_3 as the three-body interaction.

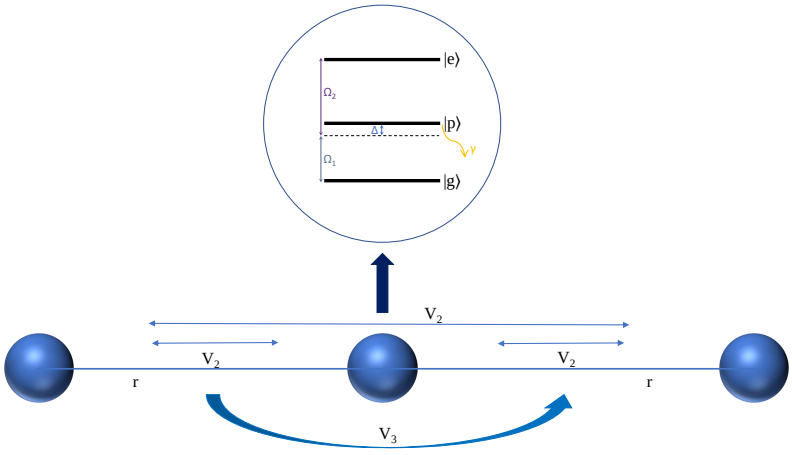

Fig. 3.34: Linear arrangement

The curve (Fig. 3.35) has some similarity with the two-body interactions. The ground-state population curve informs that most of the population is in the ground-state. Therefore, effective interaction curve should take up a soft-core potential like it does in the case of two-interacting atoms. Even though the it appears to take up a soft-core potential for $\Omega_2/2\Delta_1 < 1$, like it does in the two interacting atoms case, but the potential appears to have bumps or distortions due to three-body interactions experienced by each atom. Similarly, for $\Omega_2/2\Delta_1 > 1$, there should be one defined maximum like for the two interacting atoms, but in this case two maxima appear, which is most pronounced for $\Omega_2/2\Delta_1 = 2$. The second maxima again is due to the same reason. Similar to the equilateral triangle configuration, the ground-state population and the interaction curve shows, unlike the two-interacting case, the initial maximum occurs for $\Omega_2/2\Delta_1 = 1.1$.

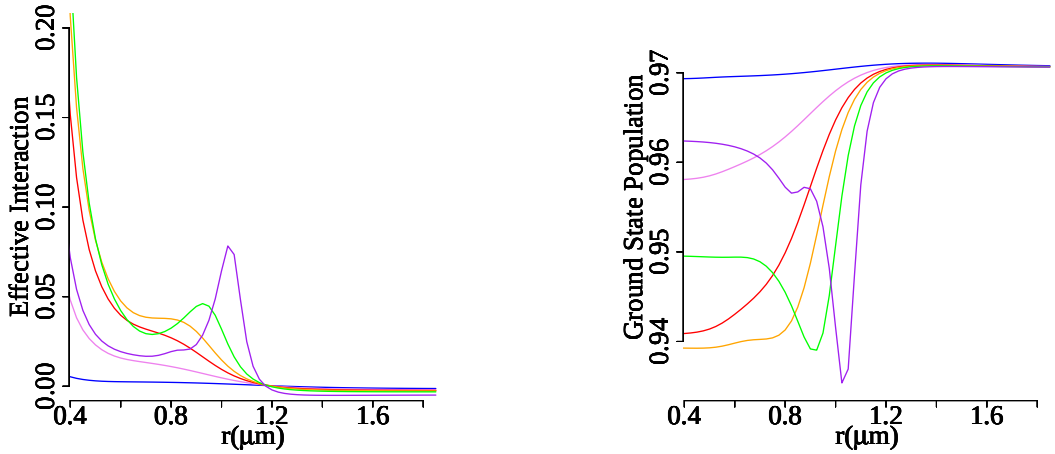

Fig. 3.35: The effective interaction and ground-state population analyzed above, are computed for $\Delta_1/\gamma_p = 2.5$, $\Omega_1/\Omega_2 = 0.1$ and varying dressing parameters $\Omega/2\Delta_1 = 0.6$ (Blue), 0.85 (Pink), 1 (Red), 1.1 (Orange), 1.3 (Green) and 2 (Purple).The decay rate γ is taken as 1. The effective interactions are scaled using the decay rate.

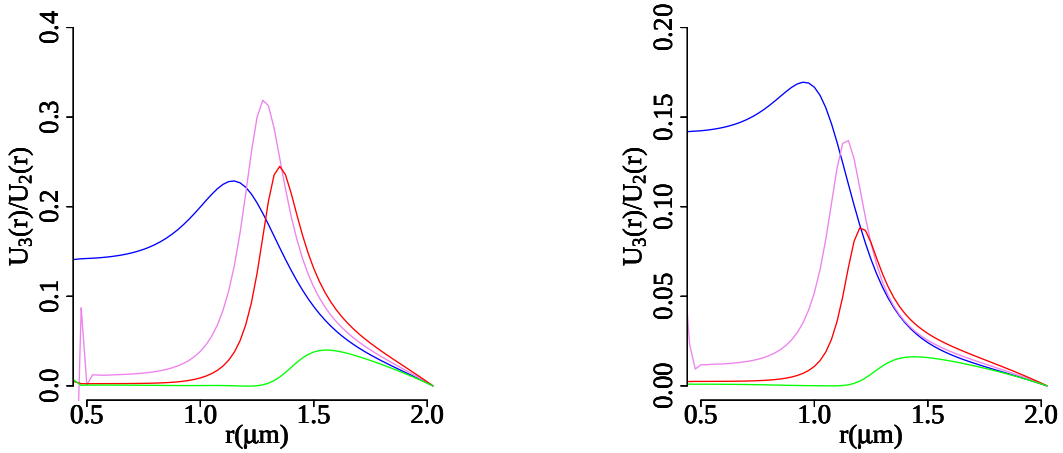

(a) Equilateral Triangle Arrangement **(b)** Linear Arrangement

Fig. 3.36: The ratio of Three–Body interactions to Two–Body interactions analyzed above for different configurations, are computed for $\Delta_1/\gamma_p = 2.5$, $\Omega_1/\Omega_2 = 0.1$ and varying dressing parameters $\Omega/2\Delta_1 = 0.6$, 0.85, 1 and 1.3.The decay rate γ is taken as 1.

3.2.2.3 Comparison of Two-Body to Three-Body Interactions

Fig. 3.36 shows that the three-body interactions are much stronger in the case of equilateral triangle. In the case of three-body interactions, the effective interactions attains a maximum for $\frac{\Omega_2}{2\Delta_1} \approx 0.6$ for small separation.

3.3 4-level Interacting atoms

In this section, the three-level interacting atoms are extended to interacting four-level atoms.

3.3.1 System

Consider two atoms, each having a four-level Λ-V ee scheme. We consider the Rydberg interactions between the two atoms in the van der Waals regime. The interaction is studied within the EIT limit and the dressing limit.

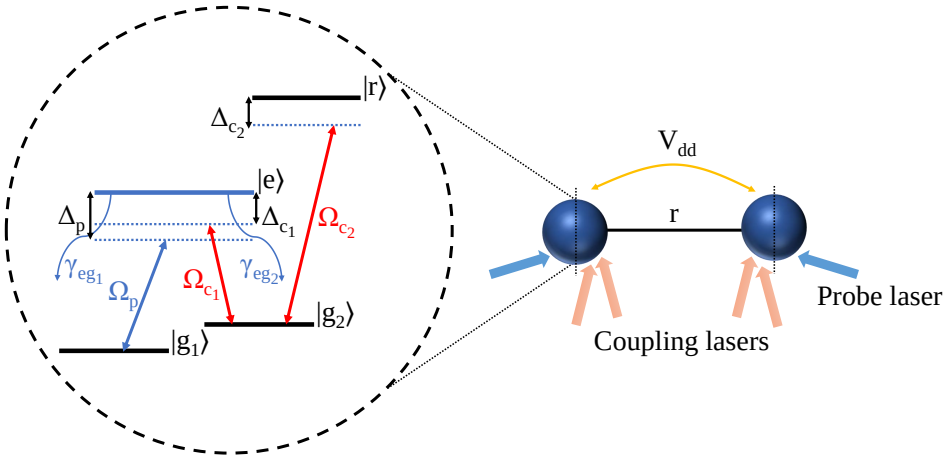

Fig. 3.37: Λ-V ee System as described by [57]

$$\text{Hamiltonian} : \mathscr{H} = \mathscr{H}^1 + \mathscr{H}^2 + \mathscr{W}_{12} \tag{3.6}$$

The one-body Hamiltonian for Λ-V ee scheme:

$$\begin{aligned}\mathscr{H}^{(i)} =& \frac{\Omega_p^{(i)}}{2}(\hat{\sigma}_{g_1e}^{(i)} + \hat{\sigma}_{eg_1}^{(i)}) + \frac{\Omega_{c_1}^{(i)}}{2}(\hat{\sigma}_{g_2e}^{(i)} + \hat{\sigma}_{eg_2}^{(i)}) + \frac{\Omega_{c_2}^{(i)}}{2}(\hat{\sigma}_{g_2r}^{(i)} + \hat{\sigma}_{rg_2}^{(i)}) \\ & - \Delta_p\hat{\sigma}_{ee}^{(i)} - (\Delta_{c_1} - \Delta_p)\hat{\sigma}_{g_2g_2}^{(i)} - (\Delta_{c_2} - (\Delta_{c_1} - \Delta_p))\hat{\sigma}_{rr}^{(i)}\end{aligned} \tag{3.7}$$

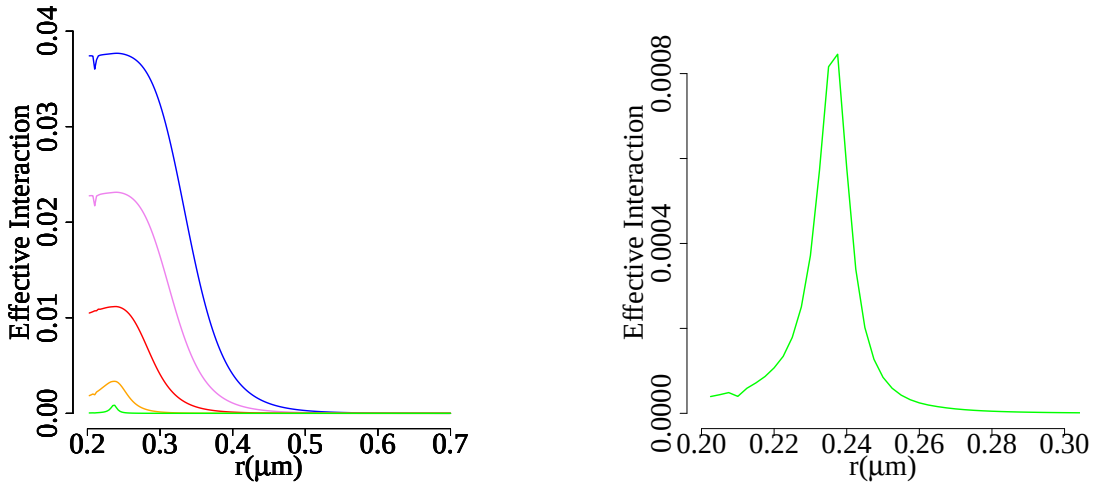

(a) Effective interaction for $\Omega/2\Delta_p = 0.2$ (Blue), 0.25 (Pink), 0.35 (Red), 0.6 (Orange) and 1(Green)

(b) Maxima of Effective Interaction for $\Omega/2\Delta_p = 1$

Fig. 3.38: The effective interactions analyzed above are computed for$(\Delta_{c_2}\text{-}(\Delta_{c_1}\text{-}\Delta_p))(\Delta_{c_1}\text{-}\Delta_p) = |\Omega_{c_2}|^2$, Δ_p/γ_e = -2.0225, Δ_{c_1}/γ_e = -2.025, $\Omega_p/\Omega_{c_1} = 0.1$, γ_r =0, $\gamma_{eg_1} = \gamma_{eg_2} = 0.5$. The decay rate γ is taken as 1. The effective interactions are scaled using the decay rate.

The effective interaction assumes a soft-core potential form very similar to those found for Rydberg-dressing of two-level atoms. There are also maxima present, as seen in the case of three-level atoms. The metastable state in our system influences the effective interaction in two ways. First, with the increase in the parameter value, the ground-state population increases, thus lowering the energy and making the maxima less pronounced in the 4-level system. Second, the metastable state also provides an additional resonance channel that leads to the kink that is seen in interaction curve (Fig. 3.38).

§

In this chapter, we extend the previously studied systems with the objective of exploring novel dynamics. A similar classification on the basis of level schemes is made as in the previous chapter — two-level, three-level, and four level schemes. In the two-level scheme, we extend the atom-light interactions for a classical field to time-dependent detuning and Rabi frequency. These extensions result in interesting dynamics — such as the formation of envelopes in the dynamics, collapse and revival of Rabi oscillations, and even oscillating steady state. The next extension for two-level atom in a classical field is to merge interaction with dissipation. Our aim for this extension was to see if the interesting dynamics seen in the presence of interaction survives for dissipative systems. We observe that while the system decays to the steady state, the envelopes appear. Finally, we extend the system to the many-atoms picture by studying the excitation dynamics, effective interaction, and multiple excitation probability. The excitation dynamics shows the existence of collapse and revival phenomenon. The effective interaction shows the decrease in plateau region as the number of atoms increase. The multiple excitation probability suggests that the blockade radius decrease as we increase the number of atoms. For a quantized field, we extend the Jaynes-Cummings model (JCM) and its extension to coher-

ent field state to two and three atoms and study the dynamics in the presence and absence of interaction. The extension of JCM to multiple atoms shows the formation of envelopes in the excitation dynamics, even in the absence of interaction — suggesting multiple coupling frequencies. We also study the effective interactions for these systems and see a similarity with the classical field case. In the three-level scheme, we extend the previous analysis of effective interaction to include angular dependence of the van der Waals interaction and three-body interaction. The angular dependence mainly shifts the previously seen effective interaction curves. The three-body interactions show a similar trend to that of the two-body interactions. We also see the importance of configuration and the significance of three-body interactions when compared to two-body interactions. Finally, we extend these schemes to four-level, where we study the effective interaction. We observe a similar trend as the three-level scheme with some new features.

4

Conclusions and Outlook

In this project, we analyzed in detail the multi-level schemes and extended to different systems. Our aim was to explore and come up with new systems in the hope of new and exciting physics. We believe that the two-level scheme, even though well studied, still has some exciting physics awaiting for us to explore, especially with Rydberg atoms. For the two-level scheme in classical field we prioritized the many-body dynamics. On the other hand for two-level scheme in a quantized field we explored the few-body dynamics for two reasons — first the extension of the Jaynes–Cummings Model from one atom to many atoms is not as trivial as it was in the case of a classical field and second, not much is explored when it comes to the quantized field, hence providing us with a wide scope for research. In the three-level scheme, our focus was on exploring the effective interaction between interacting atoms, as it has some exotic features. On the other hand its excitation dynamics is similar to that of the two-level scheme. Finally, we extended this system to a four-level scheme.

4.1 Two-level Scheme — Classical field

To begin with, we examined the two-level scheme. A two-level atom in a classical field shows the famous Rabi oscillation. This oscillation modifies to form envelopes in the presence of interaction. Keeping this in mind, we first explored the systems of an atom in a classical field with time-dependent detuning and an atom in a classical field with a time-dependent Rabi frequency. The time-dependent detuning gave rise to time-dependent amplitude oscillations of the oscillating states. It provided us with a way to alter the extent of suppression of the excited state population as a function of time. Another interesting observation, is the oscillating steady state. In a system of time-dependent detuning, the steady states oscillate with time. We did a similar analysis for time-dependent Rabi frequency. This led to us observing collapse and revival of Rabi oscillations in a classical field. Again, in this system we observed oscillating steady state with the addition of a constant detuning. A similar behavior was seen for two atoms. With a simple cosine time-dependence, we attained some interesting results in the two systems studied, and hence we conclude this has immense potential in providing novel dynamics if unique and complex functions are chosen for time-dependence. This system motivated us in finding

and exploring other systems that could provide us with a collapse and revival of Rabi oscillations. We had seen the formation of envelopes in the excitation dynamics of interacting atoms, hinting that with the increase in the number of atoms the excitation dynamics can provide some interesting results. Before extending to many-body system, we first analyzed and concluded that the envelope behavior remains intact in the presence of dissipation establishing that even in a dissipative setup the physics of the interacting atoms can be studied. Finally, we extended the system to the many-body system. Here, we studied the excitation dynamics, effective interaction, and multiple excitation probability. The excitation dynamics showed the presence of the collapse and revival behavior with the increase in the number of atoms providing us with another system for such dynamics and hinted the possible application of this system in quantum information. The effective interaction for different number of atoms showed the trend of decreasing plateau region and the nature of the soft-core potential with the increase in the number of atoms. This also led us to believe that one of the possible reasons for not being able to observe a soft-core potential in an ensemble of atoms could be the decreasing plateau region and hence the misleading appearance of the divergent nature of the potential for short separations. We concluded our work on classical field by observing the decrease in the blockade radius as the number of atoms increased. [47]. In the future, we plan to work on exploring the many atoms excitation dynamics in the presence of weak interaction. This system as we saw can be used to reproduce the dynamics attained for coherent field state. The collapse and revival behavior is used for analyzing entanglement and has applications in quantum information science. Therefore, the many atoms system with weak interaction can be used as an alternative to coherent field state.

4.2 Two-level Scheme — Quantized field

While studying the quantized field, we started with much simpler, yet interesting excitation dynamics. We began with analyzing a simple extension of the Jaynes–Cummings model to two atoms in a cavity. We observed new dynamics of the ground state population in the presence of few photons, unique to the quantized field. To explore more in this direction, we added a weak detuning to the system, the results were envelope behavior similar to the ones previously seen in the excitation dynamics in the presence of interaction. This behavior is only true of weak to intermediate values of detuning. The moment the detuning is taken to be large, the excitation dynamics show the Rabi oscillations. The addition of interaction to this system did not provide us with any new dynamics. Hence, we concluded our analysis of two atoms in quantized field and extended this system to three atoms. The three atoms dynamics showed the presence of envelope behavior for resonant transitions and it was explained as the presence of multiple Rabi frequencies. This system was analyzed in the presence of detuning and interaction in the hope of any new dynamics, but the dynamics did not change much upon addition of these parameters. We then extended our above analysis of atoms in a quantized field to atoms in

a coherent field state. The presence of a coherent field state already generates a collapse and revival behavior. The aim while studying this system was to examine how it modifies with the addition of detuning and interaction. We saw the addition of detuning only altered the amplitude of oscillation — it reduced it. On the other hand, the addition of interaction induced other frequencies, and we could see breaking of existing envelopes and formation of new and smaller envelopes. The interaction was considered weak in our studies, as the strong interaction destroyed the collapse and revival dynamics. Finally, we extended the quantized field picture to analyze dressed effective interactions and multiple excitation probability and compare them with effective interaction and multiple excitation probability attained in the classical picture. We see that the effective interaction attained in the classical picture is stronger than the ones attained for quantized and coherent field. We also showed that the blockade radius for all the three fields are same. Using the knowledge of the blockade radius, we concluded that the universal scaling exponent for the three fields are same [21]. In the future we plan extend our analysis of atoms in a quantized field to many atoms picture. We have mentioned this before, that the Rydberg atoms become interesting when we start studying many atoms. Till now our analysis were limited to three atoms, we plan to extend it to many atoms system and derive a general expression for the Hamiltonian of N atoms. In the case of classical field the dynamics became interesting when the number of atoms are increased, so we hope to see novel dynamics in many atoms interacting with quantized field.

4.3 Three-level interacting atoms

In the three-level atoms, the recent study of the effective interaction in Rydberg dressed electromagnetically induced transparency (EIT) setup saw the existence of exotic curves, appearance of maximum at finite separation [46]. We reproduced and studied these exotic curves. We then examined the effect of the angular dependence that arises due to the Rydberg state being of the form *np* to get an angular dependence of C_6 [53]. Using the numerical method mentioned in the previous chapters, the total interaction energy was calculated, and for simplicity the C_6 coefficient was taken to have only sine dependence. The result suggested that the angular dependence just shifts the curve. This behaviour was expected, as the angular dependence just decreased the C_6 value. This provided us with the method of manipulating the position of the maximum in the three-level effective interaction plot. We then went on to examine the effect of interaction in three-body systems. Two kinds of interactions are experienced by the atoms — two-body interaction [46] and 3-body interaction (see Fig. 3.32).

The effective interaction and ground-state population vs separation for the equilateral triangle is seen in Fig. 3.33 and for the linear arrangement vs separation in Fig. 3.35. The energy plot appeared similar to the two-interacting atoms. The secondary maximas are more pronounced for equilateral triangle than for the linear arrangement. Hence, the three-body interactions are more significant in the case of equilateral triangle arrangement. To confirm this, we analyzed

the the ratio of three-body effective interaction to two-body effective interaction for the two configurations. It gave us three insights. First, the equilateral triangle configuration leads to stronger three-body interactions. Second, the three-body interaction are significant when compared to two-body interaction and can lead to interesting dynamics. Finally, the potential trend of three-body is similar to the the two-body interaction. With this we concluded our three-level scheme analysis and extended the system to four-level. In the future, we plan to explore more of the three-body interactions. The three body interactions are an interesting system to explore, till now our analysis are limited to understanding the trend of the three-body interactions, importance of configuration and significance of three-body interactions when compared to two body interactions. We still have a lot of dynamics to explore, and see possible applications that we plan to study in the future.

4.4 Four–level interacting atoms

The 4-level scheme (Fig. 3.37) was investigated. We studied the effective interaction of the atoms in dressed EIT setup like the three-level picture. Unlike the three-level scheme, the four-level scheme has the third level as the metastable state. This state influences the effective interaction in two ways. With the increase in the parameter value, the ground-state population increases. This lowers the energy and makes the maxima less pronounced in the 4-level system. The metastable state also provides an additional resonance channel that leads to the kink that is seen in Fig. 3.38. The four-level dynamics shows similar trends as the three-level, with some unique features, with this we concluded the four-level system. We plan to explore these features in detail, in the future and see their possible applications.

§

In this thesis, we explored different systems with a common underlying factor — Rydberg atoms. A motivation for pursuing Rydberg atoms is that the field of Rydberg physics has been gaining a lot of importance in the recent past due to its immense potential sourcing from its exaggerated properties. We have seen its immediate applications in the field of quantum information processing, such as for creating entanglements. We know that Rydberg atoms are interesting and are a promising candidate for novel dynamics when examined in different setups. Our aim, therefore, is to explore Rydberg dynamics in novel systems and examine the possibility of interesting features arising in the dynamics. For instance, our first extension of a two-level atom to a periodically driven system, i.e. time dependent detuning or time dependent Rabi frequency when studied for Rydberg atoms leads to an appearance of blockade for much smaller interaction. We know that Rydberg blockade leads to interesting physics, such as photon-photon blockade or entanglement, but to ensure the atoms are within the blockade radius, we normally have to keep the interaction quite high. Our extension enables us to study these physics in the presence of much weaker interaction. In our extension to the many-atoms

picture, we observe that the presence of interaction leads to a collapse and revival behavior. We have seen this kind of behavior appear in a system containing an atom interacting with coherent field state, and know it is useful in quantum information processing. Research has been and is currently being done in attaining this behavior for the classical field. With a simple extension to many atoms in the weak interaction regime, we observe collapse and revival behavior. Finally, when we study the effective interaction in three-level and four–level schemes, we observe the existence of exotic curves – appearance of maximum at a finite separation. These exotic effective interaction curves imply that two Rydberg atoms can self-trap themselves without the presence of an external trapping potential. We infer from our results, that Rydberg atoms can exploited in different setups to attain exciting and novel dynamics that have immense potential for future applications.

References

[1] T. F. Gallagher, *Rydberg Atoms (Cambridge monographs on Atomic, Molecular and Chemical Physics)* (1994).

[2] J.-P. Connerade, *Highly excited atoms*, Cambridge University Press (1998).

[3] R. Stebbings, *Rydberg states of atoms and molecules*, Cambridge University Press (1983).

[4] M. L. Zimmerman, M. G. Littman, M. M. Kash, and D. Kleppner, *Stark structure of the Rydberg states of alkali-metal atoms*, Physical Review A **20**, 2251 (1979).

[5] T. Pohl, H. R. Sadeghpour, and P. Schmelcher, *Cold and ultracold Rydberg atoms in strong magnetic fields*, Physics Reports **484**, 181 (2009).

[6] K. MacAdam, D. Crosby, and R. Rolfes, *n Dependence of l-Changing Collisions between He+ Ions and Na*, Physical Review Letters **44**, 980 (1980).

[7] T. Gallagher, G. Ruff, and K. Safinya, *Resonant electronic to vibrational energy transfer from Na to C H 4 and C D 4*, Physical Review A **22**, 843 (1980).

[8] J. Dexter and T. Gallagher, *Field ionization of the n= 8–15 states of sodium*, Physical Review A **35**, 1934 (1987).

[9] J. B. Balewski, A. T. Krupp, A. Gaj, S. Hofferberth, R. Löw, and T. Pfau, *Rydberg dressing: understanding of collective many-body effects and implications for experiments*, New Journal of Physics **16**, 063012 (2014).

[10] M. Saffman and T. Walker, *Analysis of a quantum logic device based on dipole-dipole interactions of optically trapped Rydberg atoms*, Physical Review A **72**, 022347 (2005).

[11] M. Saffman, T. G. Walker, and K. Mølmer, *Quantum information with Rydberg atoms*, Reviews of Modern Physics **82**, 2313 (2010).

[12] D. Jaksch, J. Cirac, P. Zoller, S. Rolston, R. Côté, and M. Lukin, *Fast quantum gates for neutral atoms*, Physical Review Letters **85**, 2208 (2000).

[13] M. Lukin, M. Fleischhauer, R. Cote, L. Duan, D. Jaksch, J. Cirac, and P. Zoller, *Dipole blockade and quantum information processing in mesoscopic atomic ensembles*, Physical Review Letters **87**, 037901 (2001).

[14] R. Heidemann, U. Raitzsch, V. Bendkowsky, B. Butscher, R. Löw, L. Santos, and T. Pfau, *Evidence for coherent collective Rydberg excitation in the strong blockade regime*, Physical Review Letters **99**, 163601 (2007).

[15] J. A. Yeazell and C. Stroud Jr, *Observation of spatially localized atomic electron wave packets*, Physical Review Letters **60**, 1494 (1988).

[16] M. Kalinski and J. Eberly, *New states of hydrogen in a circularly polarized electromagnetic field*, Physical Review Letters **77**, 2420 (1996).

[17] J. Ahn, D. Hutchinson, C. Rangan, and P. Bucksbaum, *Quantum phase retrieval of a Rydberg wave packet using a half-cycle pulse*, Physical Review Letters **86**, 1179 (2001).

[18] J.-M. Raimond, M. Brune, and S. Haroche, *Manipulating quantum entanglement with atoms and photons in a cavity*, Reviews of Modern Physics **73**, 565 (2001).

[19] S. Gleyzes, S. Kuhr, C. Guerlin, J. Bernu, S. Deleglise, U. B. Hoff, M. Brune, J.-M. Raimond, and S. Haroche, *Quantum jumps of light recording the birth and death of a photon in a cavity*, Nature **446**, 297 (2007).

[20] B. Olmos, R. González-Férez, and I. Lesanovsky, *Fermionic collective excitations in a lattice gas of Rydberg atoms*, Physical Review Letters **103**, 185302 (2009).

[21] H. Weimer, R. Löw, T. Pfau, and H. P. Büchler, *Quantum critical behavior in strongly interacting Rydberg gases*, Physical Review Letters **101**, 250601 (2008).

[22] I. Lesanovsky, B. Olmos, and J. P. Garrahan, *Thermalization in a coherently driven ensemble of two-level systems*, Physical Review Letters **105**, 100603 (2010).

[23] C. H. Greene, A. Dickinson, and H. Sadeghpour, *Creation of polar and nonpolar ultralong-range Rydberg molecules*, Physical Review Letters **85**, 2458 (2000).

[24] V. Bendkowsky, B. Butscher, J. Nipper, J. P. Shaffer, R. Löw, and T. Pfau, *Observation of ultralong-range Rydberg molecules*, Nature **458**, 1005 (2009).

[25] E. L. Hamilton, C. H. Greene, and H. Sadeghpour, *Shape-resonance-induced long-range molecular Rydberg states*, Journal of Physics B: Atomic, Molecular and Optical Physics **35**, L199 (2002).

[26] S. T. Rittenhouse and H. Sadeghpour, *Ultracold giant polyatomic Rydberg molecules: coherent control of molecular orientation*, Physical Review Letters **104**, 243002 (2010).

[27] B. DeSalvo, J. Aman, C. Gaul, T. Pohl, S. Yoshida, J. Burgdörfer, K. Hazzard, F. Dunning, and T. Killian, *Rydberg-blockade effects in Autler-Townes spectra of ultracold strontium*, Physical Review A **93**, 022709 (2016).

[28] E. Urban, T. A. Johnson, T. Henage, L. Isenhower, D. Yavuz, T. Walker, and M. Saffman, *Observation of Rydberg blockade between two atoms*, Nature Physics **5**, 110 (2009).

[29] T. E. Lee, H. Häffner, and M. Cross, *Antiferromagnetic phase transition in a nonequilibrium lattice of Rydberg atoms*, Physical Review A **84**, 031402 (2011).

[30] J. Qian, G. Dong, L. Zhou, and W. Zhang, *Phase diagram of Rydberg atoms in a nonequilibrium optical lattice*, Physical Review A **85**, 065401 (2012).

[31] A. Hu, T. E. Lee, and C. W. Clark, *Spatial correlations of one-dimensional driven-dissipative systems of Rydberg atoms*, Physical Review A **88**, 053627 (2013).

[32] T. Peyronel, O. Firstenberg, Q.-Y. Liang, S. Hofferberth, A. V. Gorshkov, T. Pohl, M. D. Lukin, and V. Vuletić, *Quantum nonlinear optics with single photons enabled by strongly interacting atoms*, Nature **488**, 57 (2012).

[33] D. Tong, S. Farooqi, J. Stanojevic, S. Krishnan, Y. Zhang, R. Côté, E. Eyler, and P. Gould, *Local blockade of Rydberg excitation in an ultracold gas*, Physical Review Letters **93**, 063001 (2004).

[34] K. Singer, M. Reetz-Lamour, T. Amthor, L. G. Marcassa, and M. Weidemüller, *Suppression of excitation and spectral broadening induced by interactions in a cold gas of Rydberg atoms*, Physical Review Letters **93**, 163001 (2004).

[35] I. E. Protsenko, G. Reymond, N. Schlosser, and P. Grangier, *Operation of a quantum phase gate using neutral atoms in microscopic dipole traps*, Physical Review A **65**, 052301 (2002).

[36] C. Ates, T. Pohl, T. Pattard, and J. M. Rost, *Antiblockade in Rydberg excitation of an ultracold lattice gas*, Physical Review Letters **98**, 023002 (2007).

[37] T. Amthor, C. Giese, C. S. Hofmann, and M. Weidemüller, *Evidence of antiblockade in an ultracold Rydberg gas*, Physical Review Letters **104**, 013001 (2010).

[38] M. Lukin and A. Imamoğlu, *Nonlinear optics and quantum entanglement of ultraslow single photons*, Physical Review Letters **84**, 1419 (2000).

[39] A. V. Gorshkov, J. Otterbach, M. Fleischhauer, T. Pohl, and M. D. Lukin, *Photon-photon interactions via Rydberg blockade*, Physical Review Letters **107**, 133602 (2011).

[40] D. E. Chang, V. Vuletić, and M. D. Lukin, *Quantum nonlinear optics — photon by photon*, Nature Photonics **8**, 685 (2014).

[41] E. A. Martinez, C. A. Muschik, P. Schindler, D. Nigg, A. Erhard, M. Heyl, P. Hauke, M. Dalmonte, T. Monz, P. Zoller, and R. Blatt, *Real-time dynamics of lattice gauge theories with a few-qubit quantum computer*, Nature **534**, 516 (2016).

[42] S. Helmrich, A. Arias, N. Pehoviak, and S. Whitlock, *Two-body interactions and decay of three-level Rydberg-dressed atoms*, Journal of Physics B: Atomic, Molecular and Optical Physics **49**, 03LT02 (2016).

[43] Y. Chougale and R. Nath, *Ab initio calculation of Hubbard parameters for Rydberg-dressed atoms in a one-dimensional optical lattice*, Journal of Physics B: Atomic, Molecular and Optical Physics **49**, 144005 (2016).

[44] J. Zeiher, R. van Bijnen, P. Schauß, S. Hild, J.-y. Choi, T. Pohl, I. Bloch, and C. Gross, *Many-body interferometry of a Rydberg-dressed spin lattice*, Nature Physics (2016).

[45] Y.-Y. Jau, A. Hankin, T. Keating, I. Deutsch, and G. Biedermann, *Entangling atomic spins with a Rydberg-dressed spin-flip blockade*, Nature Physics **12**, 71 (2016).

[46] C. Gaul, B. DeSalvo, J. Aman, F. Dunning, T. Killian, and T. Pohl, *Resonant Rydberg Dressing of Alkaline-Earth Atoms via Electromagnetically Induced Transparency*, Phys. Rev. Lett. **116** (2016).

[47] T. Pohl and P. Berman, *Breaking the dipole blockade: Nearly resonant dipole interactions in few-atom systems*, Physical Review Letters **102**, 013004 (2009).

[48] P. Lambropoulos and D. Petrosyan, *Fundamentals of quantum optics and quantum information*, volume 23, Springer (2007).

[49] G. Wu, M. Kurz, B. Liebchen, and P. Schmelcher, *Excitation dynamics of interacting Rydberg atoms in small lattices*, Physics Letters A **379**, 143 (2015).

[50] R. Dall, A. Manning, S. Hodgman, W. RuGway, K. V. Kheruntsyan, and A. Truscott, *Ideal n-body correlations with massive particles*, Nature Physics **9**, 341 (2013).

[51] B. Olmos, R. González-Férez, and I. Lesanovsky, *Collective Rydberg excitations of an atomic gas confined in a ring lattice*, Physical Review A **79**, 043419 (2009).

[52] D. A. Steck, *Quantum and atom optics*, Oregon Center for Optics and Department of Physics, University of Oregon 47 (2007).

[53] A. W. Glaetzle, M. Dalmonte, R. Nath, I. Rousochatzakis, R. Moessner, and P. Zoller, *Quantum Spin-Ice and Dimer Models with Rydberg Atoms*, Physical Review X **4** (2014).

[54] S. Grimme, J. Antony, S. Ehrlich, and H. Krieg, *A consistent and accurate ab initio parametrization of density functional dispersion correction (DFT-D) for the 94 elements H-Pu*, The Journal of Chemical Physics **132**, 154104 (2010).

[55] K. P. Heeg, M. Gärttner, and J. Evers, *Hybrid model for Rydberg gases including exact two-body correlations*, Physical Review A **86**, 063421 (2012).

[56] M. Gärttner, K. P. Heeg, T. Gasenzer, and J. Evers, *Finite-size effects in strongly interacting Rydberg gases*, Physical Review A **86**, 033422 (2012).

[57] J. Qian and W. Zhang, *Dissipation-sensitive multiphoton excitations of strongly interacting Rydberg atoms*, Physical Review A **90** (2014).